THE JOURNAL OF BIOLOGICAL CHEMISTRY VOL. 291, NO. 52, pp. 26670–26685, December 23, 2016

Structural and Functional Study of Apoptosis-linked Gene-2·Heme-binding Protein 2 Interactions in HIV-1 Production*

Received for publication, August 8, 2016, and in revised form, October 1, 2016 Published, JBC Papers in Press, October 26, 2016, DOI 10.1074/jbc.M116.752444

Jing Ma[‡§], Xianfeng Zhang[¶], Yanbin Feng[‡], Hui Zhang[‡], Xiaojun Wang[¶], Yonghui Zheng[¶], Wentao Qiao[‡§1], and Xinqi Liu[‡2]

From the [‡]State Key Laboratory of Medicinal Chemical Biology, College of Life Sciences, Nankai University, Tianjin 300071, the [¶]CAAS-Michigan State University Joint Laboratory of Innate Immunity, State Key Laboratory of Veterinary Biotechnology, Harbin Veterinary Research Institute, Chinese Academy of Agricultural Sciences, Harbin 150069, and the [§]Key Laboratory of Molecular Microbiology and Technology, Ministry of Education, College of Life Sciences, Nankai University, Tianjin 300071, China

Edited by Dennis Voelker

In the HIV-1 replication cycle, the endosomal sorting complex required for transport (ESCRT) machinery promotes viral budding and release in the late stages. In this process, the ESCRT proteins, ALIX and TSG101, are recruited through interactions with HIV-1 Gag p6. ALG-2, also known as PDCD6, interacts with both ALIX and TSG101 and bridges ESCRT-III and ESCRT-I. In this study, we show that ALG-2 affects HIV-1 production negatively at both the exogenous and endogenous levels. Through a yeast two-hybrid screen, we identified HEBP2 as the binding partner of ALG-2, and we solved the crystal structure of the ALG-2·HEBP2 complex. The function of ALG-2·HEBP2 complex in HIV-1 replication was further explored. ALG-2 inhibits HIV-1 production by affecting Gag expression and distribution, and HEBP2 might aid this process by tethering ALG-2 in the cytoplasm.

The endosomal sorting complex required for transport (ESCRT)[3] machinery functions in HIV-1 budding and release in the late stages of viral replication (1–3). In this process, ALIX (ALG-2 interacting protein X) and TSG101 (tumor susceptibility gene 101), components of ESCRT-III and ESCRT-I, are recruited to the budding site of HIV-1 through interactions with HIV-1 Gag p6 (4–8). This promotes the release of virion particles (9) with the help of AAA-ATPase VPS4B (vacuolar protein sorting 4 homolog B) (10, 11). The penta-EF-hand protein ALG-2 (apoptosis-linked gene-2, also known as PDCD6) participates in the process by interacting with both ALIX (12, 13) and TSG101 (14) in a calcium-dependent manner and bridges ESCRT-III and ESCRT-I through dimerization (15–17). However, the function of ALG-2 in viral replication, especially that of HIV-1, remains unknown.

ALG-2 was first identified in a functional screen for anti-apoptotic proteins involved in T-cell receptor, Fas, and glucocorticoid-induced cell death (18). It was defined as a proapoptotic molecule because expression of its antisense strand led to rescue from cell death (19). However, ALG-2 knock-out mice are viable and exhibit normal T-cell development (20), which suggested that other redundant proteins might exist in mammalian cells. ALG-2 is a penta-EF-hand protein (13, 15), containing five repeats of the EF-hand motif, and coordinates three calcium ions via EF1, EF3, and EF5. However, the coordination of calcium by EF5 is weak and may be physiologically unimportant. ALG-2 exists as a dimer, which might be critical for its function as an adaptor molecule in signal transduction (15). ALG-2 can interact with dozens of proteins through several pockets (pockets 1–3) on its molecular surface. The binding motif for ALG-2, designated as the ALG-2-binding site (ABS), is a short sequence rich in Pro, Gly, and Tyr. Two typical ABS sequences have been described. ABS-1, which is represented as PPYP*XX*PGYP (*X* represents any residue) and occupies pocket 1 on the ALG-2 surface, is found in ALIX and PLSCR3 (6), whereas ABS-2, containing a P*X*PGF sequence that binds pocket 3, is found in SEC31 and PLSCR3 (15, 21). Despite being rich in Pro, Gly, and Tyr, many ALG-2 binding partners do not have a typical ABS. The crystal structures of ALG-2 bound with peptides of both motifs, derived from ALIX and SEC31, respectively, are available (12, 15, 22). In both cases, the Pro and the subsequent aromatic residues (Tyr/Phe) are critical for this interaction. The complex structures of ALG-2 with ABS peptides provide useful information concerning interactions between ALG-2 and its binding partners, whereas the lack of a full-length complex structure limits our understanding of the conformational changes induced by interactions of ALG-2 partners on both ALG-2 and its partners.

To identify new binding partners of ALG-2, a yeast two-hybrid screen was conducted with ALG-2 as the bait. HEBP2 (heme-binding protein 2, also known as SOUL) was identified repeatedly in the screen. Such an interaction has been reported in previous screenings (23, 24), but no details of this interaction are available. HEBP2 is distinct from other ALG-2 binding partners in that it lacks a canonical ABS sequence. HEBP2 is highly

* This work was supported by National Key Project on Major Infectious Diseases from the Ministry of Science and Technology Grants 2012ZX10001-008 and 2012ZX10001-006 and National Natural Science Foundation of China Grants 31370925 and 31640024.The authors declare that they have no conflicts of interest with the contents of this article.

The atomic coordinates and structure factors (code 5GQQ) have been deposited in the Protein Data Bank (http://wwpdb.org/).

[1] To whom correspondence may be addressed. Tel.: 86-22-23500950; E-mail: wentaoqiao@nankai.edu.cn.

[2] To whom correspondence may be addressed. Tel.: 86-22-23505130; E-mail: liu2008@nankai.edu.cn.

[3] The abbreviations used are: ESCRT, endosomal sorting complex required for transport; ABS, ALG-2-binding site; BisTris, 2-[bis(2-hydroxyethyl) amino]-2-(hydroxymethyl)propane-1,3-diol.

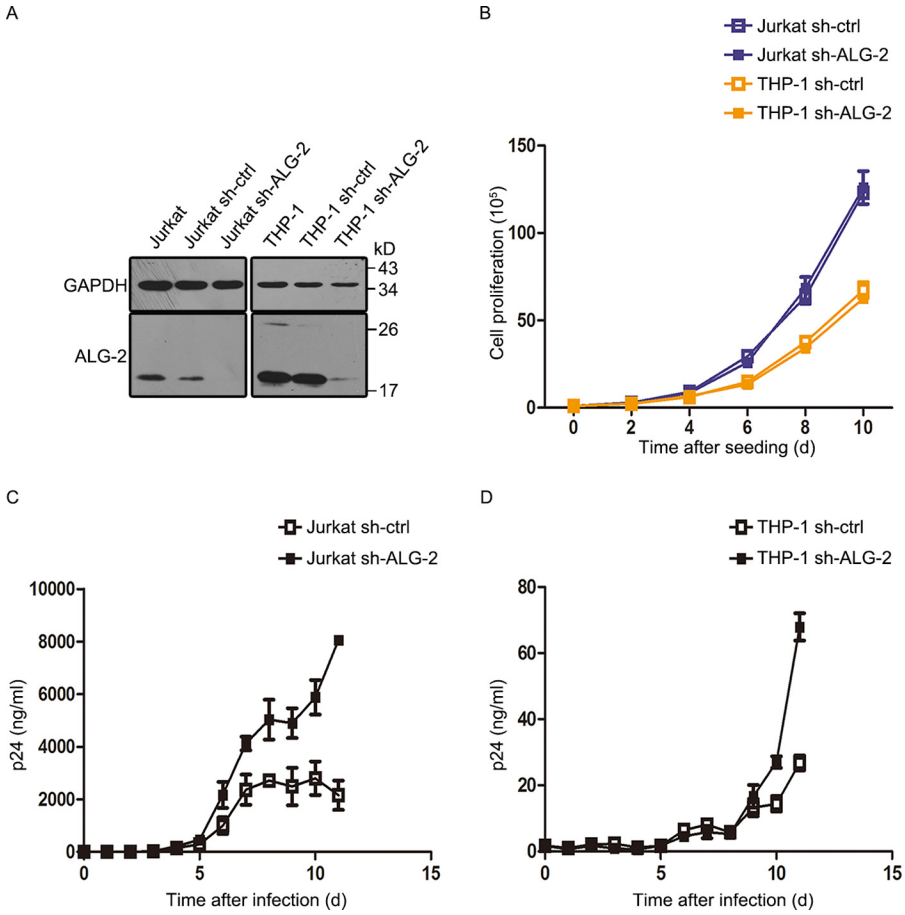

FIGURE 1. **Knockdown of endogenous ALG-2 expression in Jurkat and THP-1 cells increases HIV-1 replication.** *A,* retroviral shRNA knockdown of ALG-2 expression in Jurkat and THP-1 cells. Immunoblot images of the levels of ALG-2 and GAPDH are shown. *B,* cell proliferation of ALG-2 knockdown Jurkat and THP-1 cells (*closed squares*) or the control cells (*open squares*). The assay was started with 100,000 cells. Data are mean ± S.D., $n = 3$ technical replicates. *C* and *D,* multiple-round virus replication in ALG-2 knockdown Jurkat and THP-1 cells (*closed squares*) or the control cells (*open squares*). Jurkat and THP-1 cells were infected with 5 ng of p24 antigen of NL 4-3 viruses. Supernatants were harvested at the indicated times, and virus replication was monitored using p24 ELISA. Data shown are representative of three independent experiments.

expressed in the retina and pineal gland (25) and shares 40% sequence similarity with $p22^{HBP}$ (HEBP1), a ubiquitously expressed heme-binding protein. It has been suggested that HEBP2 plays roles in mitochondrion-mediated cell death (26), which might be related to its ability to interact with the anti-apoptotic proteins Bcl-2/Bcl-xl through a BH3-like motif (27, 28). Unlike $p22^{HBP}$, the ability of HEBP2 to bind heme is controversial, and its roles in heme-related activities, such as the generation of reactive oxygen species, are poorly defined. The involvement of HEBP2 in HIV-related activities was suggested in a recent report (29) showing that HIV Tat up-regulates HEBP2 expression. However, the mechanism underlying this effect is unknown.

In this study, the role of ALG-2 in HIV-1 production was first confirmed in HIV-1 tropic Jurkat and THP-1 cells by multiple-round viral replication. Then, based on the crystal structure of ALG-2·HEBP2, the roles of ALG-2 and HEBP2 in HIV-1 replication were investigated using a pseudotyped HIV-1 production assay. From the crystal structure of ALG-2·HEBP2 complex, we observed an interaction that differed from that of the canonical ALG-2/ABS motif, and a striking conformational change was observed on ALG-2 upon HEBP2 binding. This is the first report to establish a direct link between ALG-2·HEBP2 complex and HIV-1 production.

Results

ALG-2 Is a Cellular Inhibitor of HIV-1 Production—ALG-2 is known to interact with the ESCRT components ALIX and TSG101, and ESCRT is involved in HIV-1 production; therefore, we speculated that ALG-2 might also affect HIV-1 production. A previous report showed that ALG-2 has no dramatic effect on HIV-1 replication in either HeLa or 293T cells using a pseudovirus system (30); however, no function of ALG-2 in HIV-1 tropic cells has been tested. To address this, we used HIV-1 tropic cells, *i.e.* Jurkat cells, a leukemia T cell line, and THP-1, a monocyte cell line, to test ALG-2's function in HIV-1 multiple-round replication. ALG-2 was depleted successfully in both Jurkat and THP-1 cells using a retroviral shRNA (Fig. 1*A*), and this depletion had no discernible effect on cell proliferation (Fig. 1*B*). Interestingly, after incubation for 12 d, the HIV-1 titer was significantly higher in both cell types following ALG-2 knockdown (Fig. 1, *C* and *D*), suggesting that ALG-2 has a considerable inhibitory effect on HIV-1 replication in physiologically relevant cells.

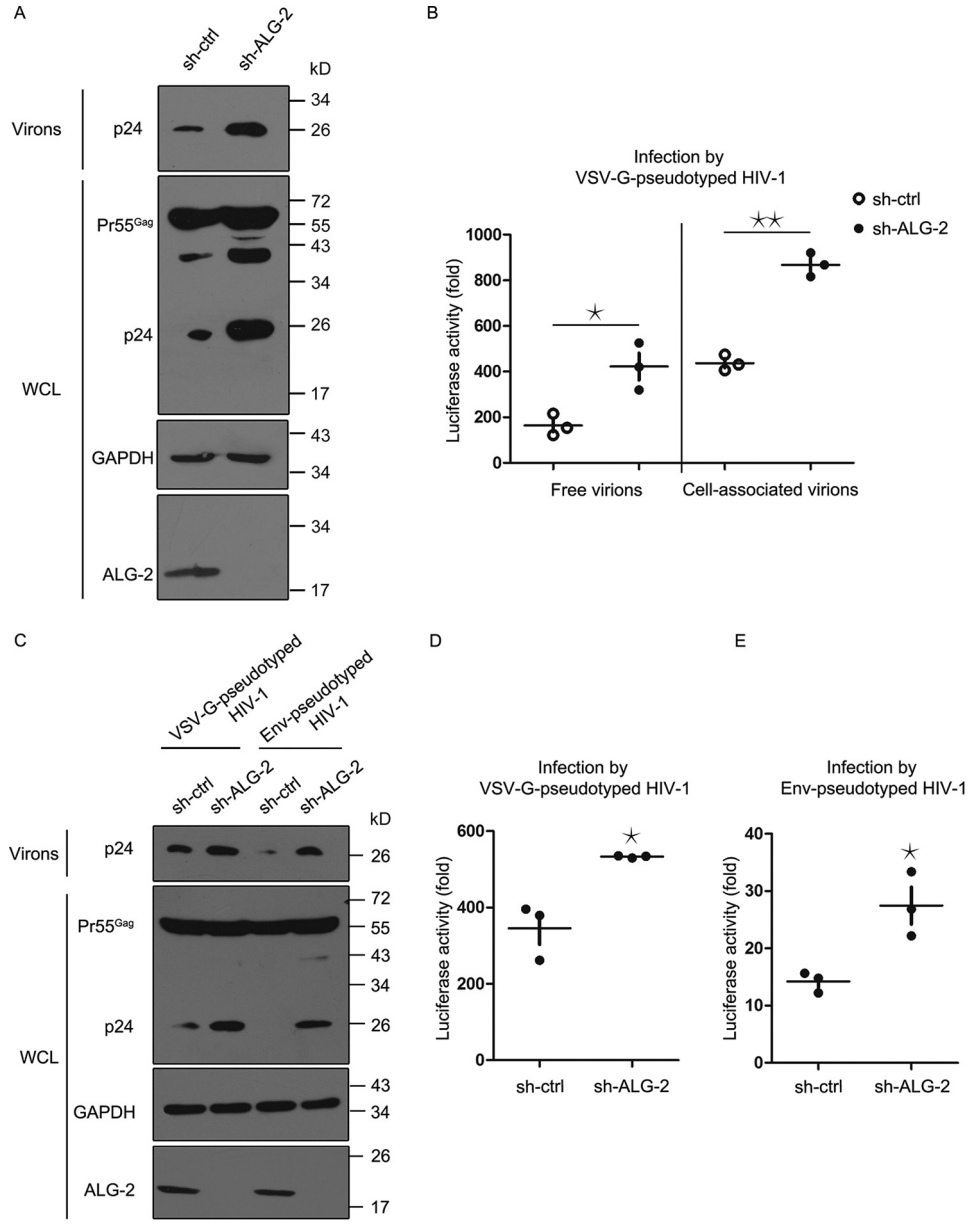

FIGURE 2. **Knockdown of endogenous ALG-2 expression in HeLa or 293T cells increases pseudotyped-HIV-1 production.** *A,* VSV-G-pseudotyped HIV-1 production was performed in ALG-2 knockdown HeLa cell lines or control cells. Virus particles in the supernatant and viruses producing cells were analyzed by Western blotting. Immunoblot images of the levels of Gag, ALG-2, and GAPDH are shown. *B,* TZM-bl cells were infected with viruses prepared in and co-cultured with virus-producing cells in *A*. After 48 h, luciferase activities were measured. (Mean ± S.D. of three technical replicates.) *, $p < 0.05$, and **, $p < 0.001$, compared with the control sample using an independent *t* test. *C,* VSV-G or Env-pseudotyped HIV-1 production was performed in ALG-2 knockdown 293T cell lines or control cells. Virus particles in the supernatant and viruses producing cells were analyzed by Western blotting. Immunoblot images of the levels of Gag, ALG-2, and GAPDH are shown. *D* and *E,* TZM-bl cells were infected with viruses prepared in *C*. After 48 h, luciferase activities were measured. (Mean ± S.D. of three technical replicates.) *, $p < 0.05$, compared with the control sample using an independent *t* test.

The knockdown of *ALG-2* by siRNA during transient expression might be incomplete (~80% according to Bregnard *et al.* (30)); therefore, we further established stable knockdown cell lines of both HeLa and 293T cells using the shRNA. Using HIV Env- or VSV-G-pseudovirus, we tested the influence of ALG-2 on HIV-1 production (Fig. 2). The titer of Env-enveloped virus in HeLa cells was too low to detect and was omitted. In both cells, depletion of ALG-2 led to higher viral production, which was more significant in HeLa cells than in 293T cells (Fig. 2, *B, D,* and *E*). By comparison of the band intensities of $Pr55^{Gag}$ and p24, total $Pr55^{Gag}$ increased in HeLa cells but was not discernible in 293T cells (Fig. 2, *A* and *C*). In both cell types, the increase in p24 was obvious upon ALG-2 depletion, indicating that ALG-2 might be involved in multiple steps of HIV-1 production, ranging from Gag expression to Gag processing. The established knockdown cell lines were also used to detect the influence of ALG-2 on viral infection, using VSV-G-pseudovirus (Fig. 3). Notably, in both Jurkat and THP-1 cells, ALG-2 depletion had no significant effect on Gag expression following one-cycle infection by the pseudovirus (Fig. 3, *A* and *B*), which was also true in HeLa and 293T cells (Fig. 3, *C* and *D*).

ALG-2 Inhibits HIV-1 Production in an ALIX/TSG101-independent Manner—ALG-2 interacts actively with ALIX and TSG101, both of which are important for HIV-1 production

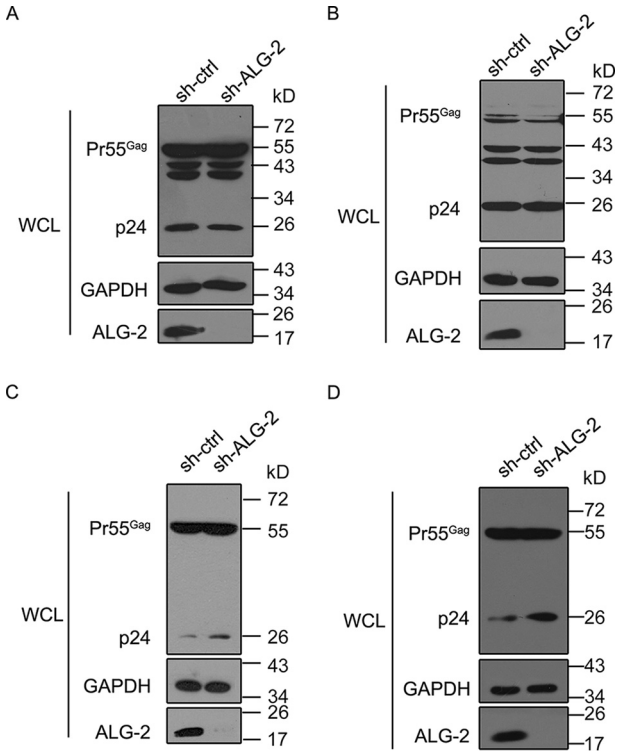

FIGURE 3. **Knockdown of ALG-2 expression in Jurkat, THP-1, HeLa, or 293T cells has no significant effect on pseudotyped HIV-1 infection.** VSV-G-pseudotyped HIV-1 was produced in 293T cells, and virions in the supernatant were harvested and used to infect ALG-2 knockdown Jurkat (*A*), THP-1 (*B*), HeLa (*C*), or 293T (*D*) and control cells. The whole cell lysates (*WCL*) were analyzed by Western blotting. Immunoblot images of the levels of Gag, ALG-2, and GAPDH are shown.

(4–8). Accordingly, we investigated whether these interactions contribute to the suppression of HIV-1 production by ALG-2. ALG-2 has a natural splicing isoform, ALG-$2^{\Delta GF}$, which lacks residues Gly^{121}-Phe^{122} and does not interact with ALIX and TSG101 (31). ALG-$2^{\Delta GF}$ had a stronger ability to suppress HIV production than ALG-2 when overexpressed in ALG-2 knockdown HeLa and 293T cells (Fig. 4, *A*–*D*), indicating the interactions with ALIX and TSG101 are not critical for ALG-2's function in HIV-1 production. ALG-2 interacts with its diverse partners to carry out its distinct role; therefore, we postulated ALG-2 might have new partners to coordinate its influence on HIV-1 production. To address this, using ALG-2 as bait, a yeast two-hybrid screen was carried out to identify potential ALG-2-interacting molecules. As a result, HEBP2 was identified.

Crystal Structure of ALG-2·HEBP2 Complex—The interaction between ALG-2 and HEBP2 was also reported in a large scale protein/protein interaction study (23). HEBP2 is distinct from other ALG-2 binding partners in lacking an identifiable ABS. To date, only crystal structures of short peptides derived from ALIX and SEC31 complexed with ALG-2 have been reported, and structures of the full-length complex of ALG-2 and its binding partners are lacking. To investigate the ALG-2·HEBP2 complex interaction in detail, we co-expressed and purified ALG-2·HEBP2 complex in the presence of calcium. The full-length ALG-2·HEBP2 complex was crystallized, and high resolution data were collected successfully (Table 1). The overall structure of the complex comprised a tetramer containing two molecules of each protein (Fig. 5*A*). ALG-2 dimerized through EF5, as reported previously (Fig. 5*B*) (13). The occupancy of three calcium ions in each ALG-2 was traced to EF1, EF3, and EF5, respectively, with poor occupation of EF5. These observations are consistent with previous reports of their ionic affinities for the three EF-hands (13). Interestingly, the sites at which HEBP2 binds to ALG-2 differ completely from that of a canonical ABS. Each HEBP2 contacts two ALG-2 molecules concomitantly around the loop between EF1 and EF2. Two residues with large side chains, Phe^{100} in HEBP2 and Trp^{57} in ALG-2, anchor to a hydrophobic pocket of the matching molecules and contribute the majority of the binding forces (Fig. 5*C*). Notably, the Phe^{100} site in HEBP2 is similar to the interaction of SEC31 with ALG-2 (22). The interacting interface between HEBP2 and ALG-2 is ~960 $Å^2$, which is much larger than that of ALIX and ALG-2 (~580 $Å^2$). To verify this interaction, mutations of F100A and W57A were introduced, and their influences on the formation of ALG-2·HEBP2 complex were detected using a pull-down assay (Fig. 5*D*). As expected, single mutations had a considerable effect on this interaction, and double mutations resulted in almost complete disruption of the complex. The interaction between ALG-2 and HEBP2 was calcium-dependent, and could be disrupted by the presence of EGTA (Fig. 5*D*).

Compared with the crystal structures of ALG-2 and HEBP2 individually, the interaction of ALG-2·HEBP2 in a complex induces conformational changes in both molecules. For HEBP2, the orientation of the loop around Phe^{100} changes to accommodate the interaction of ALG-2; however, no significant change could be found beyond this site (Fig. 6*A*). In ALG-2, the interaction with HEBP2 leads to a striking overall conformational change, especially in the dimerization region around EF5 (Fig. 6, *B* and *C*). The anti-parallel β-sheets of EF5 are distorted, and consequently, the calcium ion coordinated by EF5 has a low occupancy (*B*-factor ~100 $Å^2$) with poor electron density. When the anti-parallel β-sheets of EF5 are placed horizontally and 3D structures are projected onto the paper surface (top view), by aligning the first monomer, the second monomer in ALG-2 dimer is rotated by ~25° in the complex, and the crevice between two ALG-2 monomers becomes smaller. Compared with the dimer structure of free ALG-2 or complexed with the ALIX peptide, the ALG-2 dimer in the ALG-2·HEBP2 complex showed a more compact conformation (Fig. 6, *D*–*F*). The width of the crevice between the two monomers in the complex was reduced to 7.4 Å, compared with 23.8 Å in free ALG-2 and 30.7 Å in ALG-2/ALIX, which was reminiscent of dimeric structures in group II PEF proteins (grancalcin, sorcin, and calpain small subunit), which usually have a small crevice. Traditionally, ALG-2 was considered as a member of the group I PEF proteins, in which the dimer shows a more open conformation with a larger crevice and smaller interface formed by EF5 between two monomers. In the complex, each HEBP2 binds to two ALG-2 molecules at individual sites, and the binding forces are doubled symmetrically by two molecules of HEBP2 in the heterotetramer. ALG-2 exerts its functions by forming dimers. This reorganization of the ALG-2 dimer changes the interaction surface with other molecules, and therefore, new binding partners might be recruited by the surface formed by the ALG-2·HEBP2 interactions. The crevice

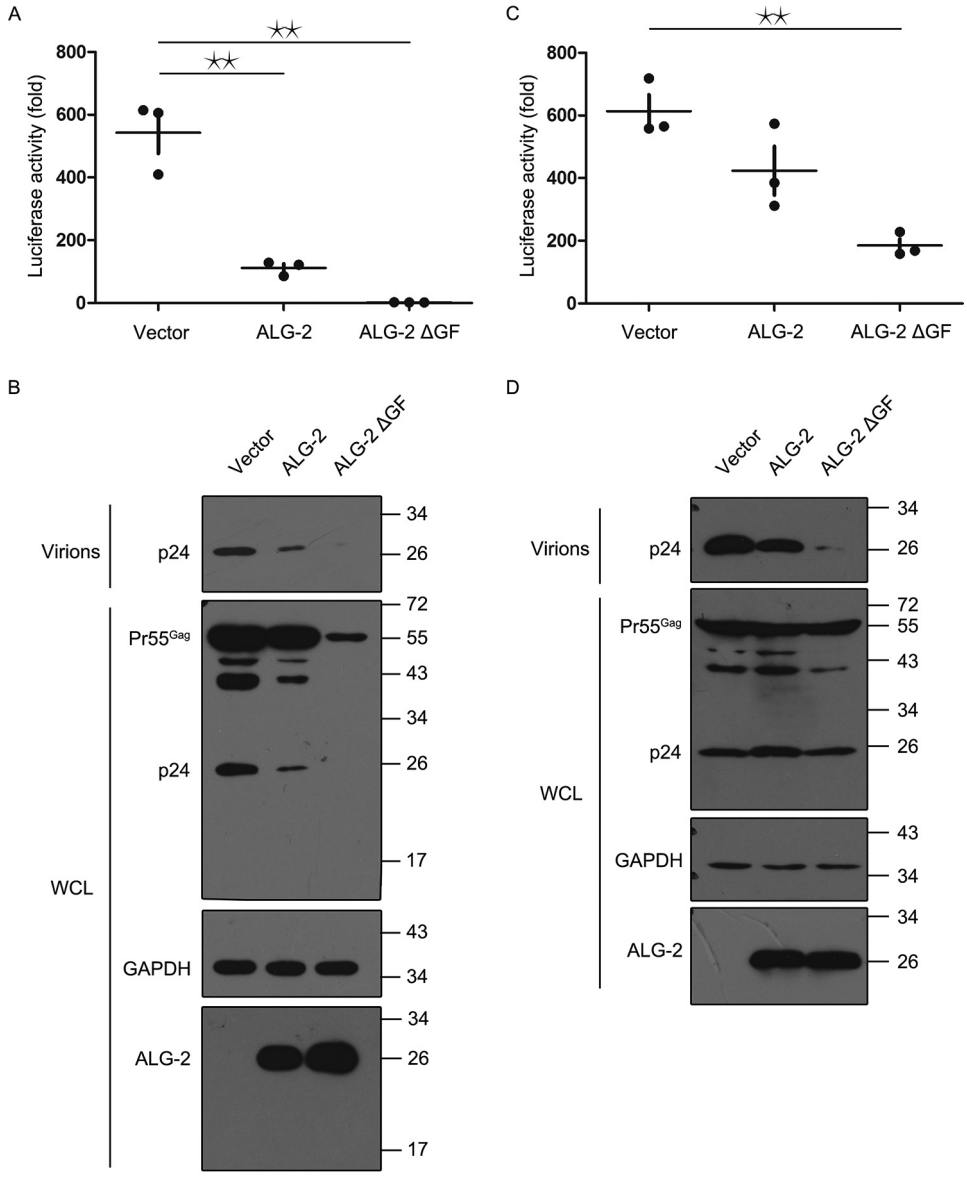

FIGURE 4. **Overexpression of ALG-2 inhibits pseudotyped HIV-1 production in an ALIX/TSG101-independent manner.** *A–D,* VSV-G-pseudotyped HIV-1 production was performed in knockdown HeLa cells (*A* and *B*) and 293T cells (*C* and *D*), with the expression of shRNA-resistant ALG-2 or ALG-2$^{\Delta GF}$. Empty vector was used as a negative control. Virus particles in the supernatant and viruses producing cells were analyzed by Western blotting. Immunoblot images of the levels of Gag, ALG-2, and GAPDH are shown in *B* and *D*. TZM-bl cells were infected with viruses prepared in HeLa (*A*) and 293T (*C*) cells. After 48 h, luciferase activities were measured. (Mean ± S.D. from three independent experiments.) **, $p < 0.001$, compared with the control sample using an independent *t* test.

between two monomers was even wider in the ALG-2·ALIX peptide complex (Fig. 6*F*), indicating the close conformation of the ALG-2 dimer induced by the interaction with HEBP2 might be specific for HEBP2, or the full-length ALIX interaction might be different from that of the ALIX peptide.

HEBP2 Interaction Changes the ALG-2 Nuclei/Cytoplasm Distribution—ALG-2 localizes to either the nucleus or the cytoplasm in a cell type- and physiology-dependent manner. In UM cells and Mel290 cells, ALG-2 localizes predominantly in the cytoplasm, with enrichment in the perinuclear region. However, in certain lung and breast cancer cells, ALG-2 shows strong nuclear staining (32). ALG-2 could also concentrate in the nucleus before cell division (33). In HeLa cells overexpressing SKD1/VPS4B^{E235Q}, ALG-2 co-localizes with the latter in aberrant endosomes around the nucleus (14). Therefore, ALG-2 might translocate between the nucleus and the cytoplasm, and its function is closely associated with its localization. ALG-2 could interact with dozens of partners in various locations; therefore, its interaction with HEBP2 might also interfere with ALG-2's localization and consequently change its function. To address this, the cellular locations of these proteins were detected by fluorescence using RFP-ALG-2 and HEBP2-GFP fusion proteins, and their co-localization was also assessed by co-expression (Fig. 7). In HeLa cells, ALG-2 was located in the entire cell, with intense fluorescence in the nucleus, whereas HEBP2 showed a diffuse distribution. Upon co-expression of HEBP2, the two proteins co-localized in puncta around the nucleus, and the intensity of ALG-2 in the nucleus decreased, indicating a cytoplasmic tethering function of HEBP2 on ALG-2 localization. Furthermore, the mutations

TABLE 1
X-ray crystallographic data and refinement statistics for ALG-2·HEBP2 complex

Data collection	
Space group	*P1*
Wavelength (Å)	0.9792
Unit cell dimensions	
a (Å)	47.28
b (Å)	78.12
c (Å)	87.17
α, β, γ (°)	113.71, 105.64, 93.95
Molecules per ASU[a]	4
Resolution (Å)[b]	30–2.20 (2.24–2.20)
Completeness (%)[b]	94.94 (91.02)
Redundancy[b]	1.90 (1.90)
No. of total reflections[b]	97,380 (5107)
No. of unique reflections[b]	51,914 (2688)
I/σ^b	18.78 (1.81)
R_{sym}(%)[b,c]	5.85 (58.10)
Figure of merit	
Refinement statistics	
Resolution (Å)	2.20
No. of reflections	51,902
R_{work}/R_{free} (%)[d,e]	19.36/23.28
No. of atoms	
Protein	5633
Water	372
Ion	8
B-Factors (Å^2)	
Protein	45.05
Water	46.33
Root mean square deviations	
Bond length (Å)	0.008
Bond angle (°)	1.129
Ramachandran analysis	
Favored (%)	95.33
Allowed (%)	3.50
Outliers (%)	1.17

[a] ASU means asymmetric unit.
[b] Values in parentheses are for the highest resolution shell.
[c] $R_{sym} = \Sigma|I - \langle I\rangle|/\Sigma\langle I\rangle$, where I is the observed intensity, and $\langle I\rangle$ is the average intensity of multiple observations of symmetry related reflections.
[d] $R = \Sigma_{hkl}||F_{obs}| - |F_{calc}||/\Sigma_{hkl}|F_{obs}|$.
[e] R_{free} is calculated from 5% of the reflections excluded from refinement.

that disrupt ALG-2·HEBP2 interactions abolished co-localization of the two proteins (Fig. 7). To confirm this, ALG-2 was expressed in HeLa cells alone or co-expressed with HEBP2, and its location was detected using nuclei/cytoplasm fractionation assays (Fig. 8*A*). As expected, ALG-2 was mostly the nuclear fraction from HeLa cells when expressed alone, but a large portion of ALG-2 was observed in the cytoplasmic fraction when co-expressed with HEBP2, and this redistribution could be abolished by mutations that disrupt ALG-2·HEBP2 interactions. Consistent with this, some HEBP2 could be translocated into the nucleus by ALG-2; however, this was not as significant as the translocation of ALG-2 (Fig. *8A*). The distribution of ALG-2 was also determined in HIV-1 tropic Jurkat cells. Both cytosolic and nuclear localization of ALG-2 was observed, with predominance in the cytosol in some but not all cells (Fig. 8*B*), indicating a varied distribution of ALG-2 in different cells.

ALG-2 Inhibits Gag Expression and Membrane Distribution—When the ALG-2 knockdown cell lines were used for HIV production in HeLa cells, the level of p24 in both supernatant and whole cell lysate increased, which was accompanied by a considerable increase in total Pr55^{Gag} (Fig. 2*A*). To determine which step is affected by ALG-2 in HIV-1 replication, the effects of ALG-2 on the HIV-1 promoter and mRNA levels were investigated (Fig. 9). ALG-2 knockdown increased the transcription from the HIV LTR promoter in HeLa cells (Fig. 9*A*). Furthermore, the level of *Pr55*^{Gag} mRNA was up-regulated by 2.7-fold following ALG-2 knockdown in HeLa cells (Fig. 9*C*). These observations suggested that ALG-2 inhibits HIV-1 transcription and leads to less Gag expression within HeLa cells, which was consistent with the amount of Pr55^{Gag} detected by Western blotting. By contrast, the effect of ALG-2 knockdown on the transcription from LTR and *Pr55*^{Gag} mRNA expression in 293T was not as significant as that in HeLa cells (Fig. 9, *B* and *D*), suggesting diverse cellular factors might be involved in the two different cell types.

In HeLa cells, upon ALG-2 depletion, the increase in *Pr55*^{Gag} expression was slight; although the increase in p24 was much more significant (Fig. 2*A*), indicating that the processing of Gag might be affected by ALG-2, a conclusion supported by the data from 293T cells (Fig. 2*C*). Taking the role of ALG-2 in endosome-associated trafficking into account, we postulated that Gag transportation and localization might be affected by ALG-2. To confirm this, in control and ALG-2-deficient cell lines, the cytosol was separated from the membrane fraction (together with the nuclei) to determine the intracellular localization of Gag during HIV-1 production (Fig. 10*A*). In total cell lysates, obviously higher levels of Pr55^{Gag} were detected in ALG-2 knockdown cells. Following cellular fractionation, in the membrane fraction, the increase in Pr55^{Gag} levels was more significant than that in the cytosol fraction after ALG-2 depletion (Fig. 10*B*). In summary, ALG-2 might affect Gag expression and distribution levels during viral replication, especially Gag accumulation on the plasma membrane.

To investigate the influence of ALG-2 on Gag distribution further, we expressed HIV Gag in HeLa cells, with or without co-expression of ALG-2 (Fig. 10*C*). Gag was located diffusely in the cytosol when expressed individually, with some puncta formed on or near the plasma membrane. In contrast, when co-expressed with ALG-2, considerable puncta containing Gag were observed in the perinuclear region (Fig. 10, *C* and *D*), where ALG-2 is also localized densely. Therefore, ALG-2 localization caused changes in the distribution of Gag, a phenomenon that requires further investigation.

HEBP2 Supports ALG-2 Inhibition of HIV-1 Production—Based on the crystal structure, HEBP2 forms a strong interaction with ALG-2 over a large surface. The two proteins formed a stable complex in solution and were also co-localized in cells (Fig. 7). Accordingly, the influences of HEBP2 on ALG-2 in HIV-1 production were detected by co-expression of the two proteins (Fig. 11). HEBP2 reduced Gag expression levels slightly when overexpressed. However, a much more notable decrease was observed when ALG-2 was co-expressed with HEBP2 (Fig. 11*A*). Furthermore, co-expression of the two proteins with mutations that disrupt the interaction between ALG-2 and HEBP2 led to a less noticeable decrease in Pr55^{Gag} expression than did co-expression of two wild-type proteins (Fig. 11*A*). This indicated that HEBP2 promotes the effects of ALG-2 in reducing Gag expression, which leads to a consequent reduction in virion production (Fig. 11, *A* and *B*). ALG-2 W57A showed more profound suppression than did the wild type. Mutation of Trp^{57} has been shown to interfere with ALG-2 interactions with other proteins (34). How this mutation is associated with ALG-2 function during HIV-1 production is unclear, and it implies that some other, as yet unidentified, pro-

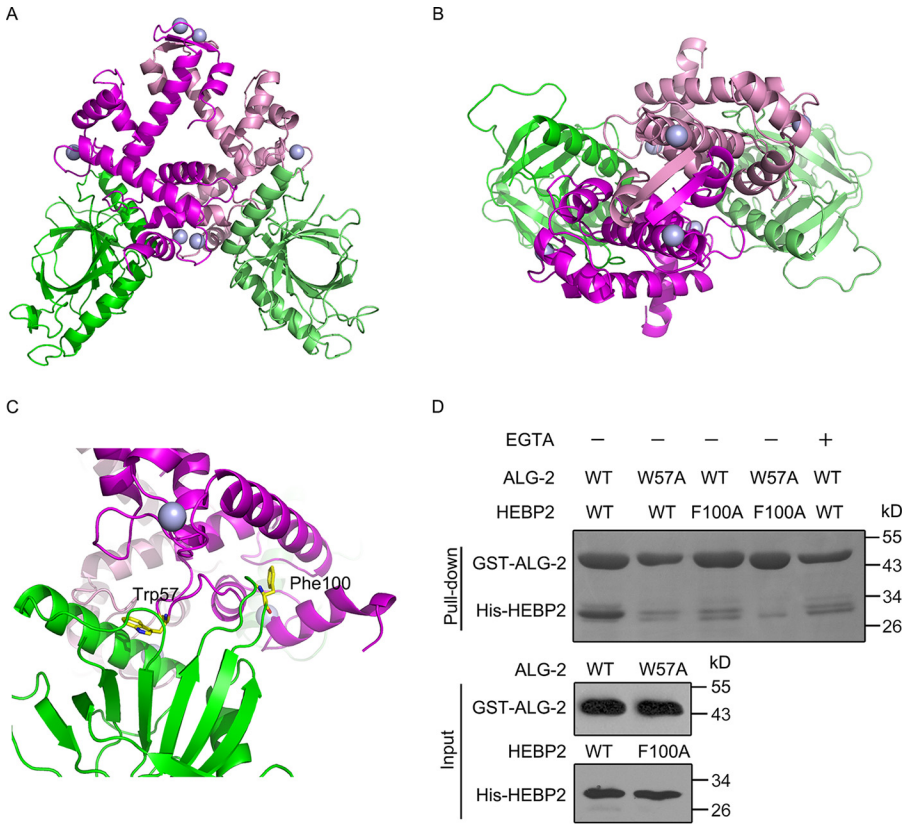

FIGURE 5. **Crystal structure of the ALG-2·HEBP2 complex.** *A,* overall view of the calcium-bound ALG-2·HEBP2 complex. ALG-2 is in *magenta* and *pink*, and HEBP2 is in *green* and *lime*. Calcium ions are shown as *light blue spheres*. Each ALG-2 molecule binds to three calcium ions. *B, top view* of the complex from above. ALG-2 forms a homodimer via anti-parallel β-strands in EF5, with HEBP2 molecules arranged on both sides. *C,* details of ALG-2·HEBP2 complex interacting interface. Two anchoring residues of Trp^{57} from ALG-2 and Phe^{100} from HEBP2 are shown by stick models and colored by atoms. *D,* for the GST pulldown assay, GST-ALG-2, HEBP2, and their mutants were obtained individually by transforming *E. coli* with plasmids. Resin-bound proteins were detected by SDS-PAGE with Coomassie Blue staining. EGTA was used to deplete calcium in *top panel, 5th lane*.

teins might be involved. In summary, these data support a suppressive effect of ALG-2 on HIV-1 production, and HEBP2 might regulate the function of ALG-2 during HIV-1 production by modulating its nuclear-cytoplasmic partitioning.

Discussion

HIV relies on the host cell machinery to complete its life cycle. During the late stage of packaging and budding, ESCRT components, of which ALIX and TSG101 are the best characterized, play critical roles. We speculated that, as an adaptor protein that interacts with ALIX and TSG101 (15–17), ALG-2 might be involved in HIV production. Knockdown of ALG-2 had considerable effect on HIV-1 replication in Jurkat and THP-1 cells. Accordingly, overexpression of ALG-2 inhibited HIV-1 production in both HeLa and 293T cells. Interestingly, ALG-2 restricted HIV-1 production by disturbing Gag expression and membrane distribution. ALG-2 is involved in vesicular trafficking (35–39) via its interactions with ALIX and TSG101 and co-localization with VPS4B (14). Therefore, it is reasonable to speculate that ALG-2 might affect Gag trafficking within the cytosol. Our data also showed that the HIV LTR and $Pr55^{Gag}$ mRNA levels were both disturbed by ALG-2 in HeLa cells, and the expression level of Gag proteins was affected consequently. This observation was consistent with a partial nuclear localization of ALG-2. Collectively, ALG-2 might affect HIV-1 production at both the mRNA and protein levels.

ALG-2 can interact with dozens of binding partners, including some important players in endosome trafficking and cell apoptosis, such as ALIX and TSG101. In this report, we found that ALG-2 forms a stable tetramer with HEBP2. Lacking the characteristic ABS motif in its sequence, HEBP2 interacts with ALG-2 differently from the ALIX/ALG-2 interaction. The crystal structure of the ALG-2·HEBP2 complex revealed a large binding surface between the two proteins, which differs from that of ALG-2 with its ABS motif in canonical ALG-2 binding partners. The interaction interface between ALG-2 and HEBP2 is distinct from the type I ABS that exists in binding partners, such as ALIX and TSG101, but overlaps partially with the type II ABS found in other binding partners, such as SEC31. Based on this, we speculated that HEBP2 might have priority in interacting with ALG-2 over other partners and thus regulate the interactions of ABS-based proteins with ALG-2. This speculation requires verification by determining the structures of ALG-2 complexed with more binding partners. To the best of our knowledge, this is the first crystal structure of ALG-2 with its binding partners using full-length proteins, which provides critical information of ALG-2 interactions with its partners beyond the ABS motifs.

Previously, Bregnard *et al.* (30) reported that ALG-2 had no dramatic effect on HIV-1 infectivity and potency in HeLa and 293T cells. Using HIV-1 tropic cells, Jurkat and THP-1, with

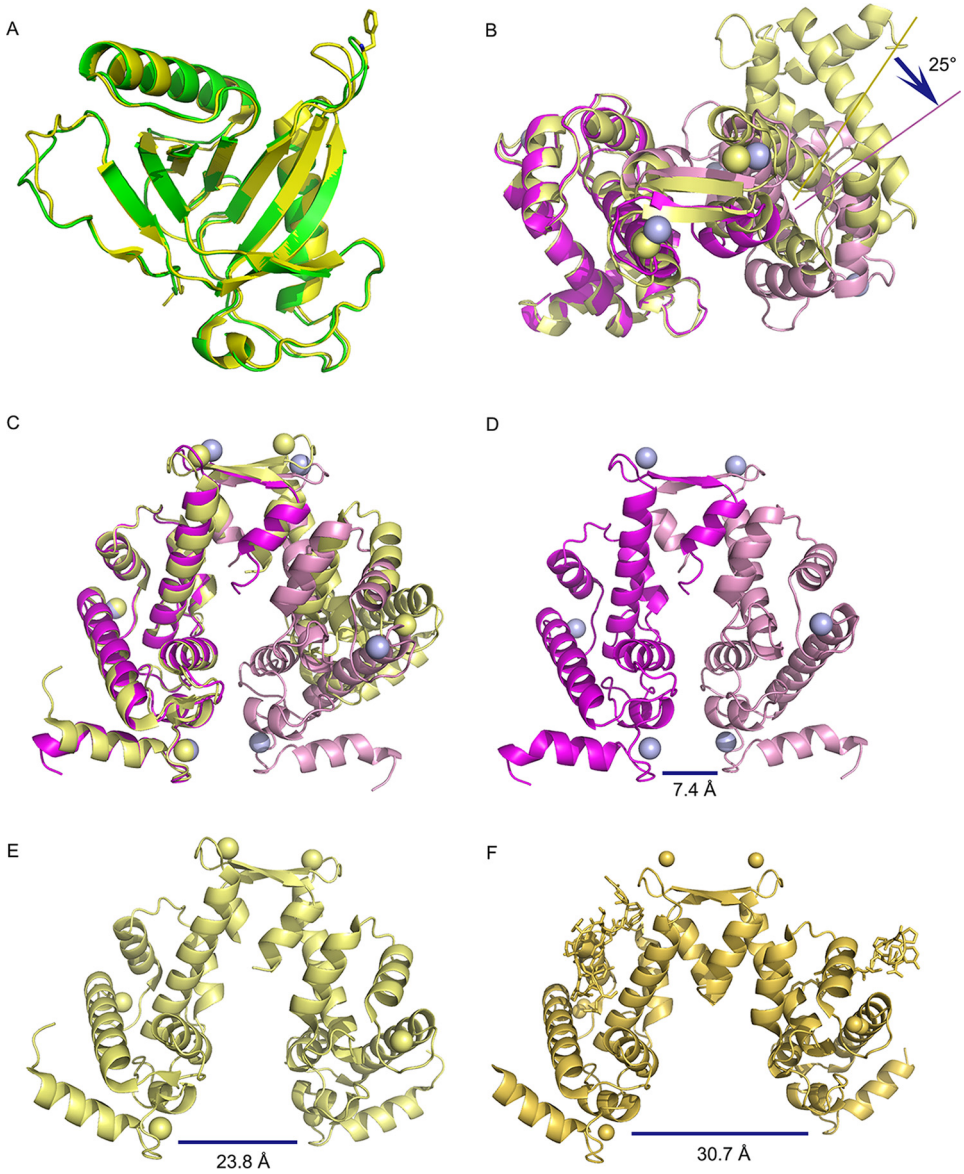

FIGURE 6. **Conformational changes induced by the ALG-2·HEBP2 complex compared with free monomers.** *A,* structural comparison between free HEBP2 and HEBP2 from the ALG-2·HEBP2 complex. The former is in *yellow* and the latter is in *green*. *B,* structural comparison between free ALG-2 dimer coordinated with calcium ions and the ALG-2 dimer from the ALG-2·HEBP2 complex. The former is in *pale yellow* and the latter is colored as in Fig. 5*A*. One of the monomers is used for superimposition. *C,* side view of *B*. *D,* side view of an ALG-2 dimer only from ALG-2·HEBP2 complex. *E,* side view of a free ALG-2 dimer coordinated with calcium ions only. *F,* side view of an ALG-2 dimer bound with ALIX peptides. The whole complex is in *yellow-orange*, and ALIX peptides are shown in stick model.

multiple-round viral replications in stable ALG-2 knockdown cell lines, we observed a considerable effect of ALG-2 on HIV-1 replication, which was supported by the observation in stable ALG-2 knockdown HeLa and 293T cell lines. The discrepancy between the two studies might have resulted from the different knockdown systems used. Bregnard *et al.* (30) used siRNA for the knockdown, with an efficiency of ~80%; some ALG-2 could still be detected on Western blots. In our study, we used shRNA to establish stable cell lines. The efficiency of knockdown was complete, and no residual ALG-2 band could be detected. The effect of ALG-2 on HIV-1 replication occurred at the late stage of HIV-1 culture, usually 5 and 8 days after initial infection in Jurkat and THP-1, respectively. This showed that ALG-2 might affect HIV-1 replication in a mild and accumulative manner, an effect that might be easily masked by high dose infection. We also noticed that the effect of ALG-2 on 293T cells was not as significant as that on HeLa cells. In addition, the effect of ALG-2 on HIV-1 infection was not obvious in the pseudoviral one-cycle infection assay. All these data suggested that the function of ALG-2 in HIV-1 production might be cell type-dependent and cellular context-dependent. Thus, they might represent an indirect effect on HIV-1 production via an influence on cell physiology rather than a direct effect on HIV-1 proteins or RNA.

ALG-2 inhibited both Env and VSV-G-pseudotyped HIV-1 production. The expression levels of Env and VSV-G were not changed in the presence or absence of ALG-2 (data not shown). It is intriguing that ALG-2 interferes with Gag expression and transportation. In most cell types, Gag is synthesized in the cytosol, myristoylated, and immediately transported to the

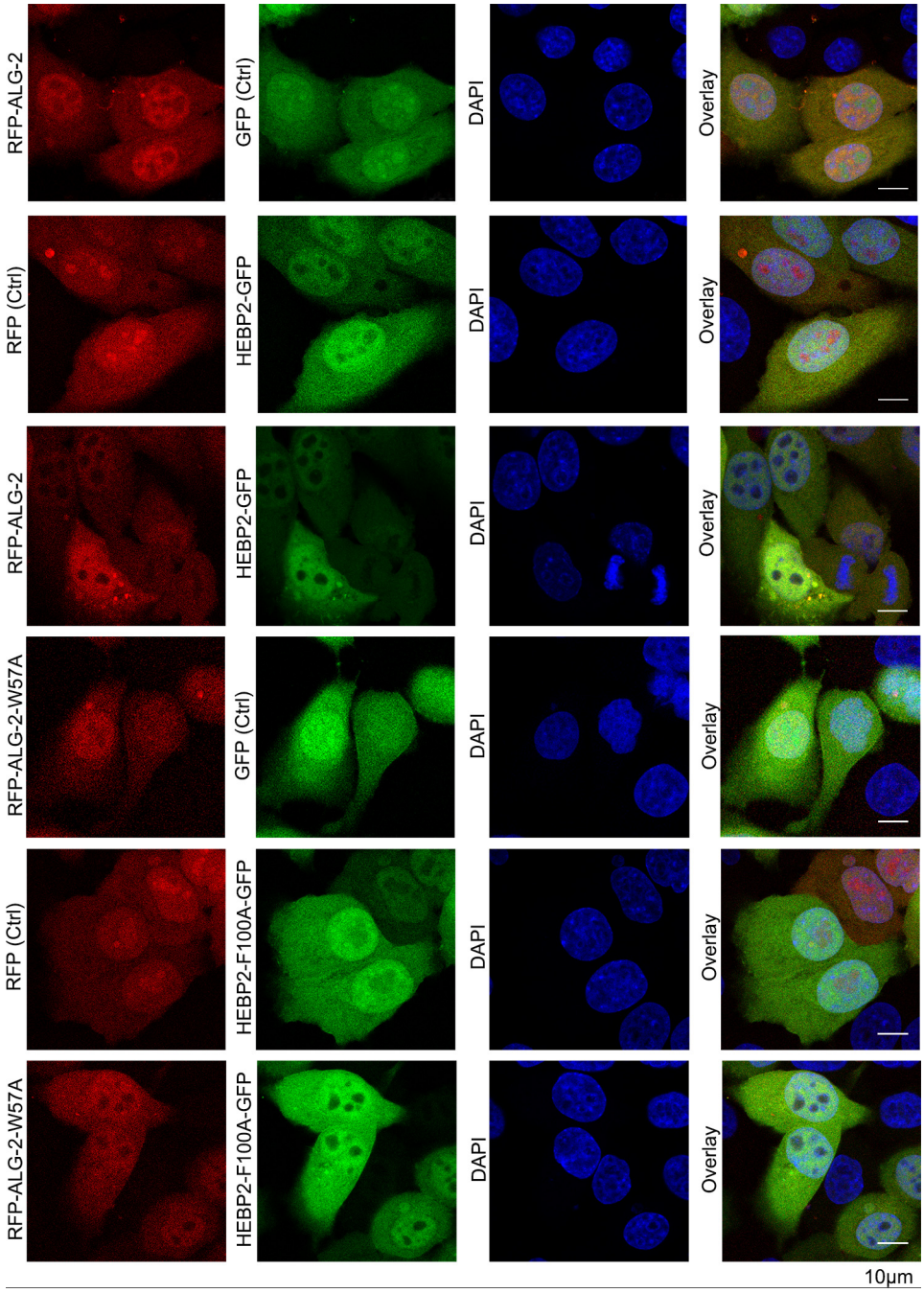

FIGURE 7. **HEBP2 co-localizes with ALG-2 in HeLa cells.** Co-localization of wild-type and mutant ALG-2 and HEBP2 in HeLa cells was investigated by confocal microscopy. The cellular distribution of RFP-ALG-2 (*red*) and HEBP2-GFP (*green*) is shown. Nuclei were stained with DAPI (*blue*). *Scale bars,* 10 μm. *Ctrl,* control.

plasma membrane. Gag found in the cytosolic vacuoles is presumed to be endocytosed from the plasma membrane (40–45). However, in macrophages, Gag might be located initially in the cytosolic vacuoles following synthesis (46, 47). A punctate location of ALG-2 was observed in the cytosol of overexpressing cells (36), and it was associated frequently with vacuoles without identifiable markers (14). How ALG-2 affects Gag membrane distribution and whether the influence is exerted following Gag synthesis or endocytosis remain to be determined. Co-expression of ALG-2 and Gag induced the formation of Gag puncta within cells, some of which co-localized with ALG-2. This observation suggested that Gag transportation is involved in the vacuole system following synthesis, at least in overexpressing cells.

The ALG-2/ALIX interaction has been suggested to play a role in endosomal trafficking and apoptosis. Our data supported the involvement of ALG-2 in HIV-1 production in an ALIX/TSG101-independent manner, because ALG-2$^{\Delta GF}$, a mutant that has lost its interactions with ALIX/TSG101, exhibited the ability to suppress HIV-1 production as the wild-type ALG-2, and the effect was even stronger (Fig. 4). Using a fusion protein of HEBP2·ALG-2 to mimic a stable ALG-2·HEBP2 complex, we also showed that HEBP2 has no influence on ALG-2 interactions with ALIX or TSG101 (Fig. 12, *top* and

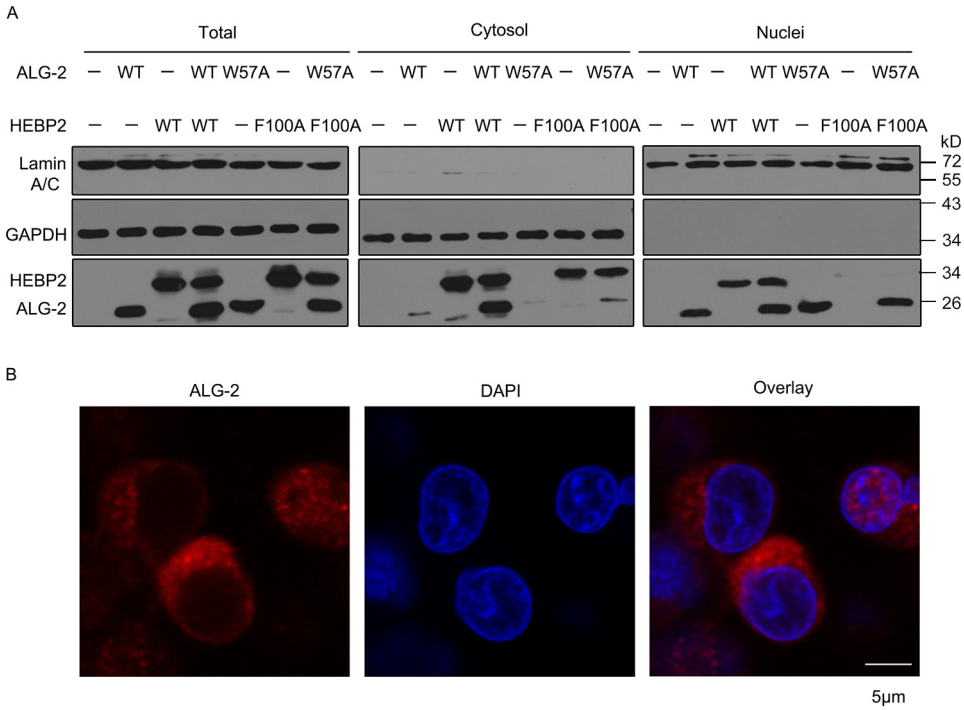

FIGURE 8. **HEBP2 interferes with ALG-2 localization via the ALG-2·HEBP2 interaction.** *A,* HeLa cells were transfected with wild-type or mutant ALG-2 and HEBP2 alone or in combination. Cell fractionation was completed to separate the nuclei (together with the membranes) from the cytosol. Each fraction was investigated by Western blotting to assess the levels of ALG-2 and HEBP2. Lamin A/C and GAPDH were used as markers of the nuclei and cytosol, respectively. *B,* Jurkat cells were transfected with ALG-2, and immunostaining was performed to analyze ALG-2 localization (*red*). Nuclei were stained with DAPI (*blue*). *Scale bars,* 5 μm.

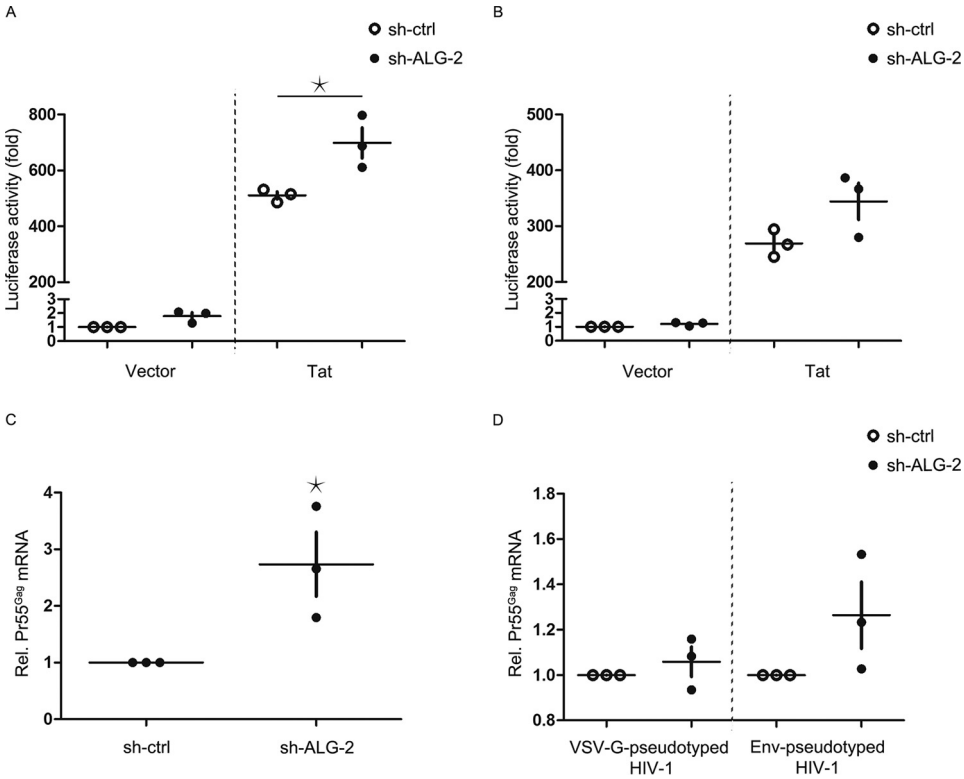

FIGURE 9. **Effects of endogenous ALG-2 on LTR transcription and *Pr55*^{Gag} mRNA expression.** *A* and *B,* transcription activity of HIV-1 LTR promoter was detected in ALG-2 knockdown HeLa cells (*A*) or 293T cells (*B*) and control cells. Cells were transfected with an HIV-1 LTR luciferase reporter plasmid, with or without HIV Tat. To normalize the transfection efficiency, pCMV-β-gal was co-transfected. The relative luciferase activity was analyzed. The luciferase activity of the control cells without Tat was arbitrarily set as 1. *C* and *D,* VSV-G-pseudotyped HIV-1 was produced in ALG-2 knockdown HeLa and control cells (*C*), and VSV-G or Env-pseudotyped HIV-1 was produced in ALG-2 knockdown 293T and control cells (*D*). Total RNA was isolated, and relative *Pr55*^{Gag} mRNA expression (normalized to *GAPDH*) was quantified using RT-PCR. *Pr55*^{Gag} mRNA expression in the control cells was arbitrarily set as 1. (Mean ± S.D. of three technical replicates.) *, $p < 0.05$ compared with the control sample using an independent *t* test.

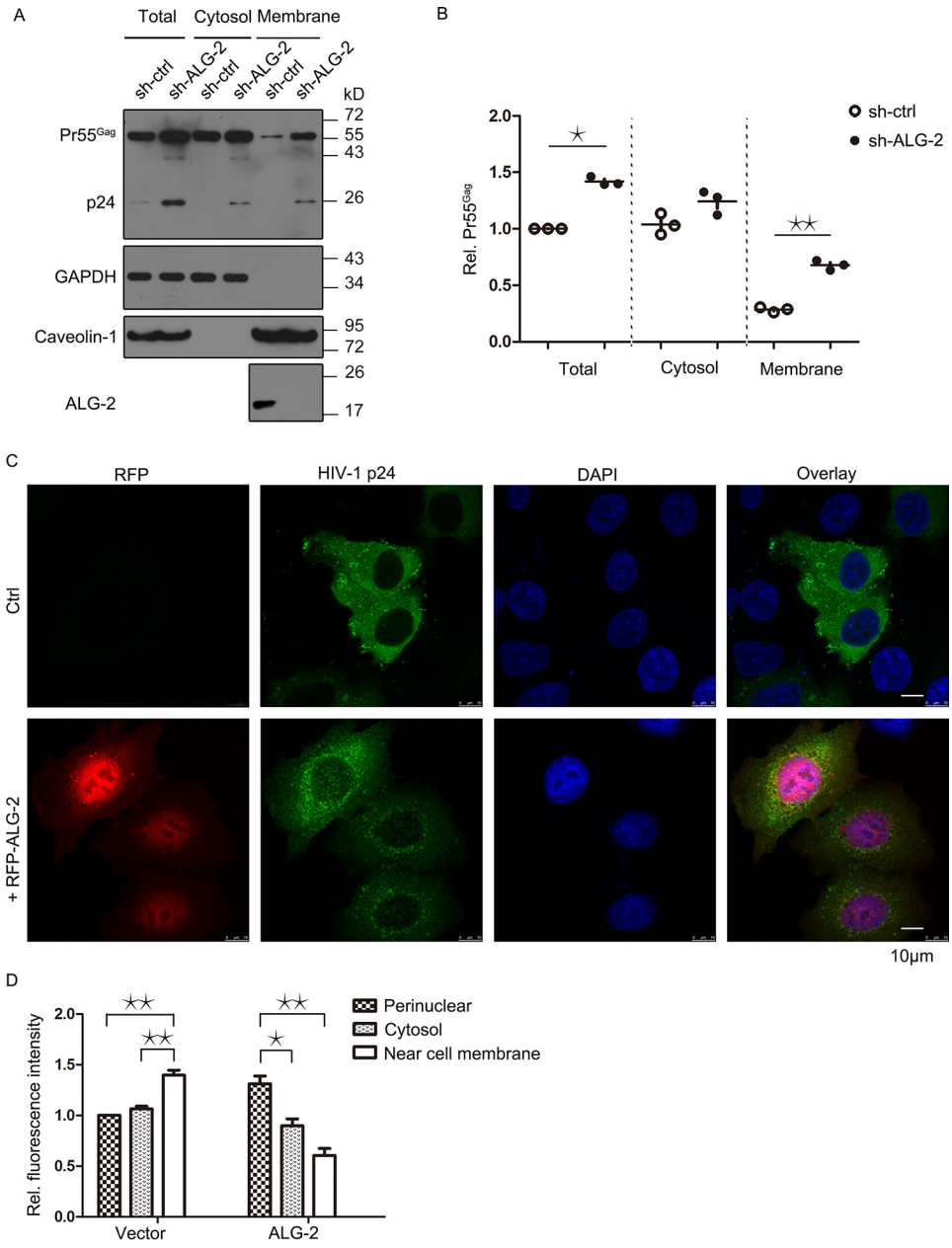

FIGURE 10. **Knockdown of endogenous ALG-2 expression in HeLa cells increases Gag expression and membrane distribution.** *A,* VSV-G-pseudotyped HIV-1 was produced in ALG-2 knockdown HeLa and control cells. Cell cytosols were separated from membranes (together with nuclei), and each fraction was analyzed by Western blotting. Immunoblot images of the levels of Gag, ALG-2, caveolin-1, and GAPDH are shown. Caveolin-1 and GAPDH were used as markers of the plasma membrane and cytosol, respectively. *B,* band intensity of $Pr55^{Gag}$ in *A* was quantified with reference to GAPDH control bands, using the ImageJ Gel Analysis program, and the relative $Pr55^{Gag}$ level is shown. $Pr55^{Gag}$ band intensity of control cells in total cell components was arbitrarily set as 1. (Mean ± S.D. from three independent experiments.) *, $p < 0.05$, and **, $p < 0.001$ compared with the control sample using an independent *t* test. *C,* overexpression of ALG-2 in HeLa cells affects HIV-1 Gag distribution. HeLa cells were co-transfected by HIV-1 Gag-Pol and HIV-1 Rev plasmid, with RFP-ALG-2 or empty vector. Confocal microscopy was performed. Cells were stained for p24 (*green*), and nuclei were stained with DAPI (*blue*). RFP-ALG-2 is shown in *red*. *Scale bars*, 10 μm. *Ctrl,* control. *D,* fluorescence intensity of Gag in *C* was quantified by the ImageJ Gel Analysis program, and the relative fluorescence intensity of Gag is shown. Three independent experiments were performed, and over 30 cells were analyzed. The fluorescence intensity of Gag in the perinuclear area in cells without ALG-2 was arbitrarily set as 1. *, $p < 0.05$, and **, $p < 0.001$ compared with the control sample using an independent *t* test.

bottom panels). Therefore, other as yet unidentified ALG-2-interacting partners might also be involved.

ALG-2 is ubiquitously expressed in nearly all tissues and organs of mammals. The physiological function of ALG-2 is not clear, although its involvement in cancer development has been reported repeatedly (48–52). ALG-2 is up-regulated in multiple cancer tissues, and it has also been reported to be down-regulated in uveal melanoma (32). However, whether ALG-2 functions as a regulator of endosomes or apoptosis in these cells remains to be determined.

Similar to ALG-2, HEBP2 is expressed ubiquitously in different tissues, despite a previous study suggesting its specificity in the retina and pineal gland (25). The estimated protein expression profile suggested that HEBP2 was overexpressed in the visceral adipose and liver secretome. This study linked HEBP2 to the vesicle transport system, in which ALG-2 is involved (22,

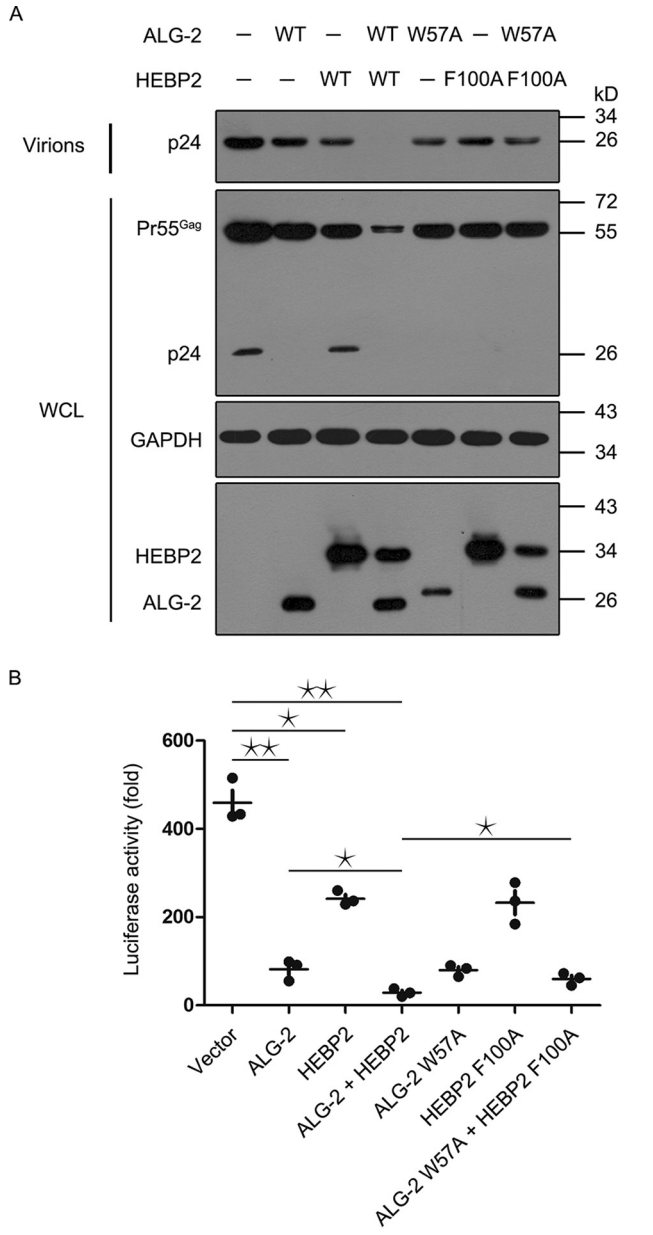

FIGURE 11. **HEBP2 promotes ALG-2 inhibition of pseudotyped HIV-1 production in HeLa cells.** *A,* VSV-G-pseudotyped HIV-1 production was performed in HeLa cells, with wild-type or mutant ALG-2 and HEBP2 expressed alone or in combination. Virus particles in the supernatant and virus-producing cells were analyzed by Western blotting. Immunoblot images of the levels of Gag, ALG-2, HEBP2, and GAPDH are shown. *B,* TZM-bl cells were infected by virions in the supernatant, and luciferase activities were measured. (Mean ± S.D. from three independent experiments.) *, $p < 0.05$, and **, $p < 0.001$ compared with the control sample using an independent *t* test.

35, 39, 53). Thus, both HEBP2 and ALG-2 might play roles in vesicle trafficking, including endosome transportation and exosome secretion. ALG-2 interacts with dozens of proteins involved in this process, including ALIX, TSG101, SEC31, ANX7, and ANX11(22).

Endogenous HEBP2 levels are low in most cell lines. However, HIV infection up-regulates the expression of HEBP2 via Tat, which might contribute to the formation of HEBP2/ALG-2 complexes within infected cells and drive HEBP2 to influence ALG-2 under physiological conditions (29).

HEBP2 has been reported as a new BH3-only protein, but considering that this proposed BH3 domain is buried and dramatic conformational changes are required to expose it for Bcl-2/Bcl-xl binding (27), this identity of HEBP2 is doubtful. HEBP2 could exaggerate the dissipation of the mitochondrial membrane potential and induce necrosis in concert with calcium (26). This suggested its involvement in intracellular calcium signaling, a process in which ALG-2 is definitely involved as an EF-hand protein. The function of both proteins in calcium signaling, together with their calcium-dependent interactions, implies their possible involvement in calcium signaling under physiological conditions.

In summary, we have established a direct link between the ALG-2·HEBP2 complex and HIV-1 production for the first time. ALG-2 has multiple effects on HIV-1 production, especially on Gag synthesis and transportation, indicating the multifunctional roles of ALG-2 inside cells. Future studies on the physiological roles of HEBP2 and ALG-2 will help to determine their functions *in vivo*.

Experimental Procedures

Plasmids and Clones—For eukaryotic expression, ALG-2, HEBP2, ALIX, and TSG101 were linked to 3×HA at the N terminus for detection by Western blotting, and ALG-2 was attached by a FLAG tag to the N terminus for co-immunoprecipitation. HA-tagged ALG-2 W57A, ALG-$2^{\Delta GF}$, and HEBP2 F100A were generated by site-directed mutagenesis using the following primers: ALG-2 W57A, 5′-CTCCAACGGCACGGCGACTCCCTTTAATC-3′ and 5′-GATTAAAGGGAGTCGCCGTGCCGTTGGAG-3; ALG-$2^{\Delta GF}$, 5′-CTGAAGCAGGCCCTCTCAGGCTACCGGCTCTCTGAC-3′ and 5′-GTCAGAGAGCCGGTAGCCTGAGAGGGCCTGCTTCAG-3′; and HEBP2 F100A, 5′-GGTTCAGGTCCTGCTAGTGAGTCTACC-3′ and 5′-GGTAGACTCACTAGCAGGACCTGAACC-3′. The shRNA-resistant ALG-2 and ALG-$2^{\Delta GF}$ were generated by site-directed mutagenesis using the following primers: 5′-ATCCAGTGACTGTGAGGTCGATCATAT-3′ and 5′-ATATGATCGACCTCACAGTCACTGGAT-3′; 5′-TGGATATGATCGAGCTCACAGTCACTG-3′ and 3′-CAGTGACTGTGAGCTCGATCATATCCA-3′. For prokaryotic expression, GST was fused to the N terminus of ALG-2, and His_6 was fused to the N terminus of HEBP2. GST-tagged ALG-2 W57A and His-tagged HEBP2 F100A were generated by site-directed mutagenesis using the primers shown above. Truncated ALG-2(23–191) and HEBP2(19–197) were constructed for crystallization.

For co-immunoprecipitation, HEBP2·ALG-2 was constructed as a FLAG-tagged fusion plasmid with HEBP2 and ALG-2 linked by a short sequence, AGGATCAGGAGGA. HEBP2-F100A-ALG-2 W57A was generated by site-directed mutagenesis using the primers shown above. RFP-ALG-2 and HEBP2-GFP were constructed for confocal microscopy analysis.

Retroviral shRNA for human ALG-2 knockdown was purchased from Origene (Beijing, China). The NLENY1-ES-IRES plasmid was a gift from Dr. David Levy (Department of Medicine, University of Alabama at Birmingham) (55).

To construct the HIV-1 LTR-luc plasmid, the HIV LTR was subcloned into a pGL3-basic luciferase reporter vector,

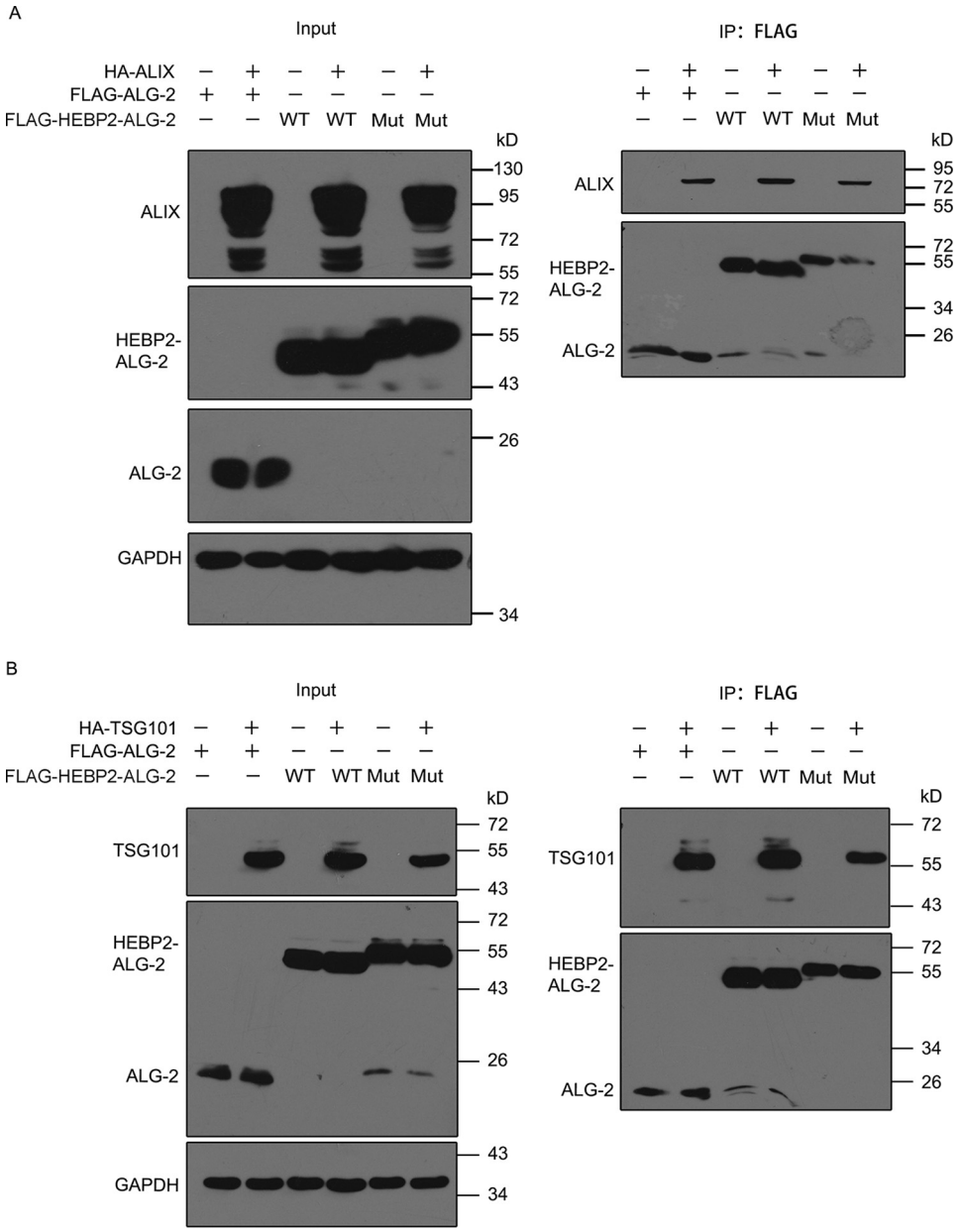

FIGURE 12. **HEBP2 does not disrupt the interactions of ALG-2 with ALIX or TSG101.** *A,* 293T cells were co-transfected with FLAG-ALG-2, wild type, or mutant (*Mut*) FLAG-HEBP2-ALG-2, with or without HA-ALIX. Cell lysates were immunoprecipitated (*IP*) with an anti-FLAG antibody and analyzed by Western blotting. Immunoblot images of the levels of ALG-2, HEBP2-ALG-2, ALIX, and GAPDH are shown. *B,* empty vector or HA-TSG101 was co-overexpressed with FLAG-ALG-2, wild type, or mutant FLAG-HEBP2-ALG-2 in 293T cells, and co-immunoprecipitation assays were performed as described in *top panel*. Western blotting was performed, and immunoblot images of the levels of ALG-2, HEBP2-ALG-2, TSG101, and GAPDH are shown.

upstream of the luciferase gene. HIV-1 Tat was constructed into a pQCXIP vector, with HA attached to the N terminus.

Protein Expression, Purification, and Crystallization—His_6-tagged HEBP2 and GST-tagged ALG-2 were co-expressed in *Escherichia coli* BL21 (DE3) strain (Novagen) and cultured in Luria-Bertani (LB) medium, supplemented with kanamycin (50 μg/ml) and ampicillin (50 μg/ml). Cells were grown at 37 °C until the A_{600} reached 0.8. Recombinant protein expression was induced by the addition of 200 μM isopropyl β-D-1-thiogalactopyranoside for 12 h at 16 °C. The cells were harvested and resuspended in binding buffer (50 mM Tris-HCl, 500 mM NaCl, pH 8.0). Harvested cells were lysed by sonication and clarified by centrifugation (38,000 × *g*, 20 min, 4 °C). The proteins were loaded onto glutathione-Sepharose resin (GE Healthcare) and eluted using elution buffer (binding buffer plus 10 mM GSH). The GST tag was removed by PreScission protease (GE Healthcare) digestion for 12 h at 4 °C. The proteins were then further purified by gel filtration (Superdex 200, GE Healthcare) in binding buffer. Fractions containing protein complexes of HEBP2 and ALG-2 proteins were pooled and concentrated to 10 mg/ml.

Crystals of the HEBP2·ALG-2 complex were grown using the sitting-drop vapor diffusion method at room temperature. 1 μl of protein solution (10 mg/ml in 50 mM Tris-HCl, 500 mM NaCl, pH 8.0) was mixed with 1 μl of reservoir solutions (0.1 M BisTris, 2 M NaCl, pH 5.5). Crystals grew to 100 × 100 × 150 μM

in 3 days using 0.2 M sodium chloride and 20% w/v polyethylene glycol 3350.

Data Collection and Structure Determination—Crystals were cryo-protected in mother liquor supplemented with 20% glycerol, and X-ray data were collected at 100 K on beamline BL17U at the Shanghai Synchrotron Radiation Facility. The diffraction data sets were processed with the HKL2000 package (56). The structure was solved by molecular replacement using PHENIX with 3R8K (HEBP2) and 2ZN8 (ALG-2) as search models (57).

Two HEBP2 and ALG-2 molecules were identified, and manual adjustments of residue positions were performed in Coot (58). The data collection and refinement statistics are summarized in Table 1, and the models were visualized and analyzed by using PyMOL.

GST Pulldown—Wild-type and mutant His_6-tagged HEBP2 and GST-tagged ALG-2 were expressed in *E. coli* BL21 (DE3) strain (Novagen) individually, and cell pellets were mixed together in a 1:1 ratio for sonication. The cell lysates were clarified by centrifugation (38,000 × *g*, 20 min, 4 °C) and then loaded onto glutathione-Sepharose resin. The proteins were collected after elution and resuspended in SDS-PAGE loading buffer. The samples were separated by SDS-PAGE, and Coomassie staining was then used to detect the interacting proteins that were captured by the resin. In Fig. 5*D*, *top panel*, *5th lane*, 5 mM EGTA was added to the binding buffer in the cell lysis process.

Cell Cultures and Transfection—HEK293T, HeLa, TZM-bl, Jurkat, and THP-1 cells were obtained from the American Type Culture Collection (ATCC). 293T, HeLa, and TZM-bl cells were cultured in Dulbecco's modified Eagle's medium (DMEM) with 10% fetal bovine serum (FBS), penicillin (50 units/ml), and streptomycin (50 μg/ml). Jurkat and THP-1 cells were cultured in Roswell Park Memorial Institute (RPMI)-1640 medium with 10% FBS, penicillin (50 units/ml), and streptomycin (50 μg/ml). Cells were incubated at 37 °C, under 5% CO_2. Cells were seeded 24 h before transfection with the plasmids using Lipofectamine 2000 (Invitrogen) or polyethyleneimine.

Construction of ALG-2 Knockdown Cell Lines—ALG-2 knockdown Jurkat, THP-1, 293T, and HeLa cell lines were produced by retrovirus transduction. Retrovirus was produced by co-transfecting 293T cells with pGFP-V-RS-shRNA, pCMV-MLV-gag-pol, and pVSV-G. Virions released into the supernatant were harvested and used to infect cells in the presence of Polybrene (5 μg/ml) by spinoculation at 1800 × *g* for 30 min at 37 °C. The stably transduced HeLa cells were selected with 2 μg/ml puromycin.

Infection of ALG-2 Knockdown Jurkat or THP-1 Cells—293T cells (2.5×10^6) were transfected with the HIV-1 proviral construct pNL 4-3 (10 μg) using polyethyleneimine. After 48 h, the supernatants were harvested. The p24 antigen levels in the viral supernatants were measured by HIV-1 p24-antigen capture ELISA. To examine virus replication, ALG-2 knockdown or control Jurkat/THP-1 cells (2×10^5) were infected with 5 ng of p24 antigen of NL 4-3 viruses. Spinfection was performed at 300 × *g* for 2 h at room temperature. Cells were washed with medium three times to remove free virions and then cultured in fresh medium. Supernatants were sampled every day, and p24 antigen production was quantified using ELISA.

Pseudotyped HIV-1 Production, Cell-free Infection, and Co-culture—NL 4-3 Env or VSV-G-pseudotyped HIV-1 was produced by co-transfecting ALG-2 knockdown 293T or HeLa cell lines with NLENY1-ES-IRES and pSRHS-Env or pVSV-G. For cell-free infection, virus particles were harvested and then used to infect TZM-bl cells; for co-culture, virus-producing cells were harvested and added to TZM-bl cells. Luciferase activities were measured after 48 h.

Cell Lysis and Western Blotting—To analyze protein levels, cells were harvested 48 h after transfection. Cells were treated with lysis buffer (0.5% Nonidet P-40, 0.1% Triton X-100, 0.1% sodium deoxycholate, 10 mM Tris-HCl, pH 8.0, 150 mM NaCl, 1 mM EDTA) containing protease inhibitors (Roche Applied Science) for 30 min on ice (59). The whole cell lysates were clarified by centrifugation (10,000 × *g*, 10 min, 4 °C). The proteins were further extracted with SDS loading buffer at 100 °C for 10 min, and then analyzed by SDS-PAGE. The protein bands were transferred to 0.45-μm PVDF membranes, blocked with 5% skim milk, and probed with primary antibodies as follows: anti-HA (Sigma, H3663); anti-GAPDH (Santa Cruz Biotechnology, sc-32233); anti-HIV-1 p24 (Millipore, Mab8790); anti-ALG-2 (Santa Cruz Biotechnology, sc-292580); anti-FLAG (Sigma, F1804); anti-caveolin-1 (Santa Cruz Biotechnology, sc-894); and anti-Lamin A/C (Santa Cruz Biotechnology, sc-7292), followed by the corresponding HRP-conjugated secondary detection antibodies as follows: goat anti-mouse IgG-HRP (Santa Cruz Biotechnology, sc-2005); goat anti-rabbit IgG-HRP (Santa Cruz Biotechnology, sc-2004). Immunoreactive proteins were detected via exposure to X-ray films.

Co-immunoprecipitation—293T cells (1×10^7 in 10-cm diameter dishes) were transfected by 6 μg of HA-tagged ALIX or TSG101, together with 4 μg of FLAG-tagged ALG-2, and wild-type or mutant HEBP2-ALG-2. After 48 h, cells were lysed by sonication in a buffer containing 150 mM NaCl, 50 mM Tris-HCl, pH 8.0, 2 mM EDTA, pH 7.4, 1% Nonidet P-40, 3% glycerol, and protease inhibitors (Roche Applied Science). The whole cell lysates were clarified by centrifugation (10,000 × *g*, 10 min, 4 °C) and then incubated with anti-FLAG antibodies for 2 h, followed by absorption onto protein A-agarose (Millipore) for 2 h. After six washes, the precipitated materials were extracted from the SDS loading buffer at 100 °C for 20 min. Proteins levels were detected by Western blotting as described previously.

Luciferase Activity Measurement—TZM-bl cells contained the luciferase reporter gene under the control of the HIV-1 LTR promoter. When infected by HIV, the LTR was transactivated by Tat, leading to luciferase expression. The luciferase activity was measured 48 h post-infection using a commercial assay system (Promega). Cells were rinsed with PBS and lysed in lysis buffer. Lysates were clarified by centrifugation (10,000 × *g*, 3 min) and then mixed with luciferin reagent, and the luciferase activity was measured using a luminometer following the manufacturer's instructions.

ALG-2 knockdown HeLa (1×10^5) or 293T (2.5×10^5) cell lines were transfected by HIV-1 LTR-luc (0.1 μg), pCMV-β-gal (0.1 μg), with or without HIV Tat (0.1 μg). After 48 h, the luciferase activity was measured as indicated. The relative luciferase activity was calculated by dividing the luciferase activity by the β-gal activity.

Immunostaining and Confocal Microscopy—HeLa cells (3×10^4/well) were seeded on glass coverslips in 12-well plates 24 h before transfection with RFP-ALG-2 or the vector, together with an HIV-1 Gag-Pol and Rev plasmid. After 48 h, cells were fixed with 4% paraformaldehyde for 10 min at room temperature (in 1× PBS) and then permeabilized with 0.1% Triton X-100 for 10 min. After blocking in 3% BSA (in 1× PBS) for 2 h, cells were stained with antibodies against HIV-1 p24 (Millipore, Mab8790) for 2 h and then probed with Alexa Fluor 647-conjugated secondary anti-mouse antibody (Molecular Probes, A21235) for 40 min. Nuclei were stained with DAPI. Similarly, Jurkat cells were stained with antibodies against ALG-2 (Abcam, ab56933) for 2 h and then probed with FITC-conjugated secondary anti-mouse antibody (Jackson ImmunoResearch, 715-095-150) for 40 min. Images were recorded using a Leica laser scanning confocal microscope (Leica TCS SP5). An Apo ×40 oil immersion objective was used, and the resolution was set to 1024 × 1024. Microscope imaging software LAS AF was used for image processing. ImageJ was then used to quantify the fluorescence intensity.

RNA Extraction and Real Time PCR—Pseudotyped HIV-1 was produced in ALG-2 knockdown HeLa and 293T cell lines. Cells were rinsed with PBS and lysed in TRIzol (Roche Applied Science) for 5 min on ice. Lysed cells were mixed with chloroform and centrifuged (10,000 × *g*, 15 min, 4 °C). The aqueous upper phase was transferred into a new tube, and isopropyl alcohol was added for RNA precipitation. Reverse transcription was performed according to the manufacturer's instructions of the RT-PCR kit (Promega). Real time PCR was completed using a two-step real time PCR kit (SYBR Green, Roche Applied Science), with the following primers: HIV-1 *Pr55*^{Gag}, 5′-AATTCGGTTAAGGCCAGGGG-3′ and 5′-TGCGAATCGTTCTAGCTCCC-3′; *GAPDH*, 5′-AACAGCGACACCCACTCCTC-3′ and 5′-CATACCAGGAAATGAGCTTGACAA-3′.

Cell Fractionation—At 48 h post-transfection, HeLa cells were rinsed with PBS and then permeabilized in digitonin solution (4 °C, 10 min) (54). After centrifugation (1000 × *g*, 4 °C, 3 min), the digitonin-solubilized material was removed and saved as the cytosolic fraction. The remaining cellular material was washed twice in ice-cold PBS and then lysed in lysis buffer as described above for Western blotting. The cell lysates were saved as the membrane fraction (together with the nuclei). Samples for each fraction were extracted with SDS loading buffer (100 °C, 20 min). Proteins were then analyzed by SDS-PAGE and Western blotting.

Author Contributions—X. L. and W. Q. conceived the project and analyzed the data. X. L. prepared most of the manuscript. X. L., W. Q., Y. Z., and X. W. designed the experiments. J. M. performed most of the experiments and prepared the manuscript with X. L. X. Z. conducted Fig. 1, *C* and *D*. Y. F. conducted Figs. 5, *A–C*, and 6. H. Z. conducted Fig. 5*D*.

References

1. Usami, Y., Popov, S., Popova, E., Inoue, M., Weissenhorn, W., and Göttlinger, H. G. (2009) The ESCRT pathway and HIV-1 budding. *Biochem. Soc. Trans.* **37,** 181–184
2. Hurley, J. H. (2015) ESCRTs are everywhere. *EMBO J.* **34,** 2398–2407
3. Bieniasz, P. D. (2009) The cell biology of HIV-1 virion genesis. *Cell Host Microbe* **5,** 550–558
4. Martin-Serrano, J., and Marsh, M. (2007) ALIX catches HIV. *Cell Host Microbe* **1,** 5–7
5. Strack, B., Calistri, A., Craig, S., Popova, E., and Göttlinger, H. G. (2003) AIP1/ALIX is a binding partner for HIV-1 p6 and EIAV p9 functioning in virus budding. *Cell* **114,** 689–699
6. Zhai, Q., Fisher, R. D., Chung, H. Y., Myszka, D. G., Sundquist, W. I., and Hill, C. P. (2008) Structural and functional studies of ALIX interactions with YPXnL late domains of HIV-1 and EIAV. *Nat. Struct. Mol. Biol.* **15,** 43–49
7. Garrus, J. E., von Schwedler, U. K., Pornillos, O. W., Morham, S. G., Zavitz, K. H., Wang, H. E., Wettstein, D. A., Stray, K. M., Côté, M., Rich, R. L., Myszka, D. G., and Sundquist, W. I. (2001) Tsg101 and the vacuolar protein sorting pathway are essential for HIV-1 budding. *Cell* **107,** 55–65
8. VerPlank, L., Bouamr, F., LaGrassa, T. J., Agresta, B., Kikonyogo, A., Leis, J., and Carter, C. A. (2001) Tsg101, a homologue of ubiquitin-conjugating (E2) enzymes, binds the L domain in HIV type 1 Pr55(Gag). *Proc. Natl. Acad. Sci. U.S.A.* **98,** 7724–7729
9. Hurley, J. H., and Hanson, P. I. (2010) Membrane budding and scission by the ESCRT machinery: it's all in the neck. *Nat. Rev. Mol. Cell Biol.* **11,** 556–566
10. Peel, S., Macheboeuf, P., Martinelli, N., and Weissenhorn, W. (2011) Divergent pathways lead to ESCRT-III-catalyzed membrane fission. *Trends Biochem. Sci.* **36,** 199–210
11. Caillat, C., Macheboeuf, P., Wu, Y., McCarthy, A. A., Boeri-Erba, E., Effantin, G., Göttlinger, H. G., Weissenhorn, W., and Renesto, P. (2015) Asymmetric ring structure of Vps4 required for ESCRT-III disassembly. *Nat. Commun.* **6,** 8781
12. Suzuki, H., Kawasaki, M., Inuzuka, T., Okumura, M., Kakiuchi, T., Shibata, H., Wakatsuki, S., and Maki, M. (2008) Structural basis for Ca^{2+}-dependent formation of ALG-2/Alix peptide complex: Ca^{2+}/EF3-driven arginine switch mechanism. *Structure* **16,** 1562–1573
13. Jia, J., Tarabykina, S., Hansen, C., Berchtold, M., and Cygler, M. (2001) Structure of apoptosis-linked protein ALG-2: Insights into Ca^{2+}-induced changes in penta-EF-hand proteins. *Structure* **9,** 267–275
14. Katoh, K., Suzuki, H., Terasawa, Y., Mizuno, T., Yasuda, J., Shibata, H., and Maki, M. (2005) The penta-EF-hand protein ALG-2 interacts directly with the ESCRT-I component TSG101, and Ca^{2+}-dependently co-localizes to aberrant endosomes with dominant-negative AAA ATPase SKD1/Vps4B. *Biochem. J.* **391,** 677–685
15. Maki, M., Suzuki, H., and Shibata, H. (2011) Structure and function of ALG-2, a penta-EF-hand calcium-dependent adaptor protein. *Sci. China Life Sci.* **54,** 770–779
16. Maki, M., Maemoto, Y., Osako, Y., and Shibata, H. (2012) Evolutionary and physical linkage between calpains and penta-EF-hand Ca^{2+}-binding proteins. *FEBS J.* **279,** 1414–1421
17. Okumura, M., Ichioka, F., Kobayashi, R., Suzuki, H., Yoshida, H., Shibata, H., and Maki, M. (2009) Penta-EF-hand protein ALG-2 functions as a Ca^{2+}-dependent adaptor that bridges Alix and TSG101. *Biochem. Biophys. Res. Commun.* **386,** 237–241
18. Vito, P., Lacanà, E., and D'Adamio, L. (1996) Interfering with apoptosis: Ca^{2+}-binding protein ALG-2 and Alzheimer's disease gene ALG-3. *Science* **271,** 521–525
19. Lacanà, E., Ganjei, J. K., Vito, P., and D'Adamio, L. (1997) Dissociation of apoptosis and activation of IL-1β-converting enzyme/Ced-3 proteases by ALG-2 and the truncated Alzheimer's gene ALG-3. *J. Immunol.* **158,** 5129–5135
20. Jang, I. K., Hu, R., Lacaná, E., D'Adamio, L., and Gu, H. (2002) Apoptosis-linked gene 2-deficient mice exhibit normal T-cell development and function. *Mol. Cell. Biol.* **22,** 4094–4100
21. Takahashi, T., Suzuki, H., Inuzuka, T., Shibata, H., and Maki, M. (2012) Prediction of a new ligand-binding site for type 2 motif based on the crystal structure of ALG-2 by dry and wet approaches. *Int. J. Mol. Sci.* **13,** 7532–7549
22. Takahashi, T., Kojima, K., Zhang, W., Sasaki, K., Ito, M., Suzuki, H., Kawasaki, M., Wakatsuki, S., Takahara, T., Shibata, H., and Maki, M. (2015) Structural analysis of the complex between penta-EF-hand ALG-2 protein

and Sec31A peptide reveals a novel target recognition mechanism of ALG-2. *Int. J. Mol. Sci.* **16,** 3677–3699
23. Rual, J. F., Venkatesan, K., Hao, T., Hirozane-Kishikawa, T., Dricot, A., Li, N., Berriz, G. F., Gibbons, F. D., Dreze, M., Ayivi-Guedehoussou, N., Klitgord, N., Simon, C., Boxem, M., Milstein, S., Rosenberg, J., *et al.* (2005) Towards a proteome-scale map of the human protein-protein interaction network. *Nature* **437,** 1173–1178
24. Rolland, T., Taşan, M., Charloteaux, B., Pevzner, S. J., Zhong, Q., Sahni, N., Yi, S., Lemmens, I., Fontanillo, C., Mosca, R., Kamburov, A., Ghiassian, S. D., Yang, X., Ghamsari, L., Balcha, D., *et al.* (2014) A proteome-scale map of the human interactome network. *Cell.* **159,** 1212–1226
25. Zylka, M. J., and Reppert, S. M. (1999) Discovery of a putative heme-binding protein family (SOUL/HBP) by two-tissue suppression subtractive hybridization and database searches. *Mol. Brain Res.* **74,** 175–181
26. Szigeti, A., Bellyei, S., Gasz, B., Boronkai, A., Hocsak, E., Minik, O., Bognar, Z., Varbiro, G., Sumegi, B., and Gallyas, F. (2006) Induction of necrotic cell death and mitochondrial permeabilization by heme binding protein 2/SOUL. *FEBS Lett.* **580,** 6447–6454
27. Ambrosi, E., Capaldi, S., Bovi, M., Saccomani, G., Perduca, M., and Monaco, H. L. (2011) Structural changes in the BH3 domain of SOUL protein upon interaction with the anti-apoptotic protein Bcl-xL. *Biochem. J.* **438,** 291–301
28. Szigeti, A., Hocsak, E., Rapolti, E., Racz, B., Boronkai, A., Pozsgai, E., Debreceni, B., Bognar, Z., Bellyei, S., Sumegi, B., and Gallyas, F., Jr. (2010) Facilitation of mitochondrial outer and inner membrane permeabilization and cell death in oxidative stress by a novel Bcl-2 homology 3 domain protein. *J. Biol. Chem.* **285,** 2140–2151
29. López-Huertas, M. R., Mateos, E., Sánchez Del Cojo, M., Gómez-Esquer, F., Díaz-Gil, G., Rodríguez-Mora, S., López, J. A., Calvo, E., López-Campos, G., Alcamí, J., and Coiras, M. (2013) The presence of HIV-1 tat protein second exon delays Fas protein-mediated apoptosis in CD4(+) T lymphocytes a potential mechanism for persistent viral production. *J. Biol. Chem.* **288,** 7626–7644
30. Brégnard, C., Zamborlini, A., Leduc, M., Chafey, P., Camoin, L., Saïb, A., Benichou, S., Danos, O., and Basmaciogullari, S. (2013) Comparative proteomic analysis of HIV-1 particles reveals a role for Ezrin and EHD4 in the Nef-dependent increase of virus infectivity. *J. Virol.* **87,** 3729–3740
31. Inuzuka, T., Suzuki, H., Kawasaki, M., Shibata, H., Wakatsuki, S., and Maki, M. (2010) Molecular basis for defect in Alix-binding by alternatively spliced isoform of ALG-2 (ALG-2DeltaGF122) and structural roles of F122 in target recognition. *BMC Struct. Biol.* **10,** 25
32. Subramanian, L., Crabb, J. W., Cox, J., Durussel, I., Walker, T. M., van Ginkel, P. R., Bhattacharya, S., Dellaria, J. M., Palczewski, K., and Polans, A. S. (2004) Ca^{2+} binding to EF hands 1 and 3 is essential for the interaction of apoptosis-linked gene-2 with Alix/AIP1 in ocular melanoma. *Biochemistry* **43,** 11175–11186
33. Krebs, J., and Klemenz, R. (2000) The ALG-2/AIP-complex, a modulator at the interface between cell proliferation and cell death? A hypothesis. *Biochim. Biophys. Acta* **1498,** 153–161
34. Shibata, H., Suzuki, H., Kakiuchi, T., Inuzuka, T., Yoshida, H., Mizuno, T., and Maki, M. (2008) Identification of Alix-type and Non-Alix-type ALG-2-binding sites in human phospholipid scramblase 3: differential binding to an alternatively spliced isoform and amino acid-substituted mutants. *J. Biol. Chem.* **283,** 9623–9632
35. Helm, J. R., Bentley, M., Thorsen, K. D., Wang, T., Foltz, L., Oorschot, V., Klumperman, J., and Hay, J. C. (2014) Apoptosis-linked gene-2 (ALG-2)/Sec31 interactions regulate endoplasmic reticulum (ER)-to-Golgi transport a potential effector pathway for luminal calcium. *J. Biol. Chem.* **289,** 23609–23628
36. Yamasaki, A., Tani, K., Yamamoto, A., Kitamura, N., and Komada, M. (2006) The Ca^{2+}-binding protein ALG-2 is recruited to endoplasmic reticulum exit sites by Sec31A and stabilizes the localization of Sec31A. *Mol. Biol. Cell* **17,** 4876–4887
37. Shibata, H., Suzuki, H., Yoshida, H., and Maki, M. (2007) ALG-2 directly binds Sec31A and localizes at endoplasmic reticulum exit sites in a Ca^{2+}-dependent manner. *Biochem. Biophys. Res. Commun.* **353,** 756–763
38. la Cour, J. M., Mollerup, J., and Berchtold, M. W. (2007) ALG-2 oscillates in subcellular localization, unitemporally with calcium oscillations. *Biochem. Biophys. Res. Commun.* **353,** 1063–1067
39. Bentley, M., Nycz, D. C., Joglekar, A., Fertschai, I., Malli, R., Graier, W. F., and Hay, J. C. (2010) Vesicular calcium regulates coat retention, fusogenicity, and size of pre-Golgi intermediates. *Mol. Biol. Cell* **21,** 1033–1046
40. Vlach, J., and Saad, J. S. (2015) Structural and molecular determinants of HIV-1 Gag binding to the plasma membrane. *Front. Microbiol.* **6,** 232
41. Jouvenet, N., Neil, S. J. D., Bess, C., Johnson, M. C., Virgen, C. A., Simon, S. M., and Bieniasz, P. D. (2006) Plasma membrane is the site of productive HIV-1 particle assembly. *PLoS Biol.* **4,** e435
42. Finzi, A., Perlman, M., Bourgeois-Daigneault, M. C., Thibodeau, J., and Cohen, É. A. (2013) Major histocompatibility complex class-II molecules promote targeting of human immunodeficiency virus type 1 virions in late endosomes by enhancing internalization of nascent particles from the plasma membrane. *Cell. Microbiol.* **15,** 809–822
43. Finzi, A., Orthwein, A., Mercier, J., and Cohen, E. A. (2007) Productive human immunodeficiency virus type 1 assembly takes place at the plasma membrane. *J. Virol.* **81,** 7476–7490
44. Harila, K., Prior, I., Sjöberg, M., Salminen, A., Hinkula, J., and Suomalainen, M. (2006) Vpu and Tsg101 regulate intracellular targeting of the human immunodeficiency virus type 1 core protein precursor Pr55gag. *J. Virol.* **80,** 3765–3772
45. Neil, S. J., Eastman, S. W., Jouvenet, N., and Bieniasz, P. D. (2006) HIV-1 Vpu promotes release and prevents endocytosis of nascent retrovirus particles from the plasma membrane. *PLoS Pathog.* **2,** e39
46. Perlman, M., and Resh, M. D. (2006) Identification of an Intracellular trafficking and assembly pathway for HIV-1 Gag. *Traffic* **7,** 731–745
47. Ono, A., and Freed, E. O. (2004) Cell-type-dependent targeting of human immunodeficiency virus type 1 assembly to the plasma membrane and the multivesicular body. *J. Virol.* **78,** 1552–1563
48. Suzuki, K., Dashzeveg, N., Lu, Z. G., Taira, N., Miki, Y., and Yoshida, K. (2012) Programmed cell death 6, a novel p53-responsive gene, targets to the nucleus in the apoptotic response to DNA damage. *Cancer Sci.* **103,** 1788–1794
49. Su, D., Xu, H., Feng, J., Gao, Y., Gu, L., Ying, L., Katsaros, D., Yu, H., Xu, S., and Qi, M. (2012) PDCD6 is an independent predictor of progression free survival in epithelial ovarian cancer. *J. Transl. Med.* **10,** 31
50. Rao, R. V., Poksay, K. S., Castro-Obregon, S., Schilling, B., Row, R. H., del Rio, G., Gibson, B. W., Ellerby, H. M., and Bredesen, D. E. (2004) Molecular components of a cell death pathway activated by endoplasmic reticulum stress. *J. Biol. Chem.* **279,** 177–187
51. la Cour, J. M., Høj, B. R., Mollerup, J., Simon, R., Sauter, G., and Berchtold, M. W. (2008) The apoptosis linked gene ALG-2 is dysregulated in tumors of various origin and contributes to cancer cell viability. *Mol. Oncol.* **1,** 431–439
52. la Cour, J. M., Mollerup, J., Winding, P., Tarabykina, S., Sehested, M., and Berchtold, M. W. (2003) Up-regulation of ALG-2 cancer tissue in hepatomas and lung. *Am. J. Pathol.* **163,** 81–89
53. la Cour, J. M., Schindler, A. J., Berchtold, M. W., and Schekman, R. (2013) ALG-2 attenuates COPII budding *in vitro* and stabilizes the Sec23/Sec31A complex. *PLoS One* **8,** e75309
54. Liu, X., and Fagotto, F. (2011) A method to separate nuclear, cytosolic, and membrane-associated signaling molecules in cultured cells. *Sci. Signal.* **4,** pl2
55. Levy, D. N., Aldrovandi, G. M., Kutsch, O., and Shaw, G. M. (2004) Dynamics of HIV-1 recombination in its natural target cells. *Proc. Natl. Acad. Sci. U.S.A.* **101,** 4204–4209
56. Otwinowski, Z., and Minor, W. (1997) Processing of X-ray diffraction data collected in oscillation mode. *Methods Enzymol.* **276,** 307–326
57. Adams, P. D., Afonine, P. V., Bunkóczi, G., Chen, V. B., Davis, I. W., Echols, N., Headd, J. J., Hung, L. W., Kapral, G. J., Grosse-Kunstleve, R. W., McCoy, A. J., Moriarty, N. W., Oeffner, R., Read, R. J., Richardson, D. C., *et al.* (2010) PHENIX: a comprehensive Python-based system for macromolecular structure solution. *Acta Crystallogr. D Biol Crystallogr.* **66,** 213–221
58. Emsley, P., Lohkamp, B., Scott, W. G., and Cowtan, K. (2010) Features and development of Coot. *Acta Crystallogr. D Biol. Crystallogr.* **66,** 486–501
59. Furuta, R. A., Nishikawa, M., and Fujisawa, J. (2006) Real-time analysis of human immunodeficiency virus type 1 Env-mediated membrane fusion by fluorescence resonance energy transfer. *Microbes Infect.* **8,** 520–532